Parameter and State Estimation of Infiltration Processes

by

Song Bo

A thesis submitted in partial fulfillment of the requirements for the degree of

Master of Science

in

Process Control

Department of Chemical and Materials Engineering

University of Alberta

Abstract

Open-loop irrigation is a common practice in agriculture which leads to excessive consumption of water resources. Closed-loop is a promising alternative to reduce water consumption and to better maintain the health of crops, which requires soil moisture information of the investigated fields. An agro-hydrological system describes the water movements between soil, crop and atmosphere. Richards equation plays an important role in the study of agro-hydrological systems. It models the water movement in soil in the vadose zone, which is driven by capillary and gravitational forces. Its states (capillary potential) and parameters (hydraulic conductivity, saturated and residual soil moistures, and van Genuchten-Mualem parameters) are essential for the accuracy of mathematical modeling, yet difficult to obtain experimentally. In this thesis, methods are developed to estimate the parameters and states of Richards equation simultaneously.

First, the estimation problem is studied on one-dimensional Richards equation with spatially and temporally homogeneous parameters. The finite difference model and augmented model of Richards equation are constructed for simultaneous estimation. In the proposed estimation approach, parameter identifiability is tested to determine the identifiable parameter sets and sensitivity analysis is used to determine the most important parameter set for estimation purpose. The minimum number of sensors to ensure the identifiability of parameters is determined by conducting maximum multiplicity method. Three common estimation schemes (extended Kalman filter, ensemble Kalman filter and moving horizon estimation) are investigated. The estimation performance is compared and analyzed based on extensive

simulations.

The estimation problem is extended to estimate the parameters and states of three-dimensional Richards equation with spatially heterogeneous and temporally homogeneous parameters. The finite difference model and augmented model of three-dimensional Richards equation are developed which include parameters of multiple types of soil. In the proposed approach, decentralized or distributed estimation scheme is proposed since the increasing number of states presented in the system. Before subsystem decomposition, observability of the original augmented system is ensured. In other words, parameter identifiability and sensitivity analysis are used to determine the significant parameter set for estimation purpose. Then, the guidelines for subsystem decomposition are introduced, which is followed by observability test on subsystems. A study of interaction between subsystems is conducted which further motivates the decentralized estimation framework. The decentralized moving horizon estimation is studied and its performance is extensively discussed.

Preface

The results presented in this thesis are part of the research that is under the supervision of Dr. Jinfeng Liu. Chapter 2 of this thesis is a revised version of S. Bo, S. R. Sahoo, X. Yin, J. Liu and S. L. Shah, "Parameter and State Estimation of One-Dimensional Infiltration Processes: A Simultaneous Approach", Mathematics 2020, 8(1), 134. I was responsible for conceptualization, simulation design and analysis as well as the manuscript composition. S. R. Sahoo assisted in design, analysis and contributed to manuscript edits. X. Yin assisted in analysis and contributed to manuscript edits. S. L. Shah contributed to manuscript edits. J. Liu was the supervisory author and was involved with the concept formation and manuscript composition and edits.

Acknowledgments

I would like to thank my supervisor, Dr. Jinfeng Liu, for his guidance and support during my graduate study. Dr. Liu was patient and supportive when I faced obstacles in research project and in my life.

I would like to thank all my colleagues from Process Systems and Control Engineering group. They were always willing to help me. Especially, thank you, Xunyuan Yin, Su Liu, Jannatun Nahar, Benjamin Decardi-Nelson, Soumya Sahoo, Jianbang Liu, Yi Zhang, Guoyang Yan, An Zhang, Bernard Agyeman, Rui Nian, and Jayson McAllister. Also I would like to thank my friends, Chaoqun Li, Jierui and Yihang Li, who gave me advices and helps on research.

I would also like to thank my parents for unconditioned support. I want to thank my lovely wife, Yu Wei. Thank you for your love, your support and patience.

I would like to gratefully acknowledge the financial support from Natural Sciences and Engineering Research Council (NSERC) of Canada.

Contents

List of Tables

List of Figures

Chapter 1

Introduction

1.1 Motivation and Research Overview

Water and food scarcities are becoming serious issues worldwide due to population growth and climate change. According to United Nations' statistics [1], approximately 70% of all available fresh water is consumed for agricultural activities, with the main consumer being irrigation. Currently, the average water-use efficiency in irrigation worldwide is about 50% as reported in Fischer et al. [2]. Therefore, it is of vital importance to improve irrigation water-use efficiency, in order to address the water crisis. Currently, it is still a common practice to use open-loop irrigation, which leads to excessive consumption of water resources. Closed-loop irrigation is a promising alternative to reduce water consumption and to better maintain the health of crops [3]. In the development of such a closed-loop irrigation system, it is important to have the soil moisture information of the entire field, which is in general very difficult to obtain. One way to overcome this challenge is to estimate the field's soil moisture based on limited sensor measurements. However, this depends on the accuracy of the agro-hydrological model. In this work, we aim to develop a systematic parameter and state estimation scheme that can provide accurate estimates of soil moisture.

Specifically, in this work, we consider simultaneous state and parameter estimation based

on agro-hydrological systems modeled using the Richards equation, which describes soil water dynamics. Richards equation is a partial differential equation (PDE) which falls in the family of porous medium equation (PME). The estimation and control problems of this kind of equation were widely studied in chemical engineering [4, 5, 6, 7] and meteorology [8, 9]. The Richards equation is essentially composed of the continuity equation and Darcys law, which is incorporated with two algebraic equations of hydraulic conductivity and capillary capacity (derivative of soil-water retention curve) [10]. The parameters of Richards equation are related to soil properties. Different approaches have been developed to estimate soil properties. Soil properties may be estimated in a soil lab by directly fitting the soil-water retention curve and hydraulic conductivity curve using collected field data of soil moisture, hydraulic conductivity and corresponding capillary pressure head [10]. However, soil properties may change over time and it would be expensive to take frequent soil samples for lab analysis especially when a big field is considered. Moreover, the hydraulic conductivity is difficult to measure. As an alternative to direct lab analysis soil parameters can be estimated indirectly based on the Richards equation and some easily-accessible field measurements such as soil moisture or capillary pressure head by minimizing the difference between measured values and model predicted values. This type of indirect approaches are referred to as inverse estimation [11]. Inverse estimation has been widely applied and its applications can be generally classified into two groups: methods based on measurements observed from one-step or multi-step outflow experiments [12, 13, 14, 15] or methods based on time-series in-situ measurements [16, 17, 18, 19, 20]. These inverse estimation methods can only estimate soil parameters but not soil moisture or capillary pressure head. Moreover, they are mainly applicable to pre-collected datasets and cannot be used for online parameter estimation.

Sequential data assimilation is another widely used approach in estimating soil parameters online, which only requires the current measurement and prior knowledge of the system. In general, it consists of two steps, which are prediction and update steps. In the first step, a dynamical system model is initialized to describe a real process. Due to the limited knowl-

edge about the process, the model may not predict the process accurately. Then, in the update step, an algorithm is designed to determine how to correct the prediction, based on field measurements and the dynamical model. Moreover, sequential data assimilation has the ability to deal with uncertainties in the measurements and the model. Particle filters (PF) [21], extended Kalman filters (EKF) [22] and ensemble Kalman filters (EnKF) [23, 24, 25, 26, 27] are common and widely used algorithms in sequential data assimilation for soil parameter estimation. Li and Ren [23] studied parameter estimation by augmenting parameters as states and used EnKF as the estimation algorithm. They also studied the possible factors that affect the performance of EnKF. In Reference [24], dual ensemble Kalman filter (DEnKF) was used to first estimate the states using a standard KF and then to estimate the parameters using an unscented Kalman filter. In Reference [25], two EnKFs were used to estimate the states and parameters, separately, which neglected the complex nonlinear interaction between states and parameters. In Reference [26], the authors compared three ensemble-based simultaneous state and parameter estimation methods, augmented EnKF, DEnKF and simultaneous optimization and data assimilation (SODA) to improve the soil moisture estimation accuracy. It concluded that the augmented EnKF was the most robust method for general conditions and SODA was better at handling complex conditions. However, it was pointed out that SODA required the highest computational resources.

However, one limitation of the above discussed methods is that they cannot handle constraints on the states or parameters and the estimation performance deteriorates when the noise is not Gaussian or the initial guess is not good. Constraints on the states and parameters are important information and may be used to significantly improve estimation performance as will be demonstrated in the simulations of this work. To address the above discussed problem, we can consider the optimization based moving horizon estimation (MHE) method, which is widely used in state estimation of nonlinear systems with explicit constraints taken into account [28].

MHE was mainly investigated within a centralized framework, with some representa-

tive results reported in [28, 29, 30, 31, 32]. Since MHE converts an estimation problem into an optimization-based problem, the computational complexity is typically much higher than that of other common estimation algorithms. Therefore, when dealing with systems/processes of medium to large scales, centralized MHE may fail to provide online estimates due to increasingly high computational load; this issue is especially significant for systems with high non-linearity like the agro-hydrological systems considered in this work. In addition to concerns about the computational load, the centralized structure that exploits one single agent to handle plant-wide tasks is not favorable from the perspectives of fault tolerance, organizational and maintenance flexibility [33, 34, 35, 36, 37]. The above considerations have motivated the use of decentralized and distributed frameworks in advanced control [38, 39, 40, 41] as well as state estimation [42, 43, 44, 45]. In a decentralized/distributed context, the overall system/process is typically divided into smaller units (subsystems), and the original estimation problem which could be large and complex is typically decomposed into smaller sub-problems, which are handled by a number of local agents instead of using a single central agent. In this way, the computational burden for each agent is eased, and the fault tolerance and maintenance flexibility can be much enhanced at the same time. While the decentralized and the distributed frameworks are inherently similar, one primary difference between them is that the local agents of a decentralized scheme are fully isolated from each other while the local agents of a distributed scheme coordinate with each other via communication during the process. As a result, a distributed architecture can be advantageous when the sub-problems have significant connections; that is, when the subsystems interact with each other significantly, since the interactions can be appropriately handled by exchanging information between the local agents [35, 36]. In literature, there have been some results on decentralized MHE (DeMHE) and distributed MHE (DMHE) designs. In [46], a DMHE scheme was developed for nonlinear systems based on the concept of sensor network. In [47, 48, 49], DMHE designs where local estimators are based on decomposed subsystems were proposed. More relevant results can be found in [42, 50, 51].

While distributed schemes can provide better overall performance as compared to their decentralized counterpart in many cases, it is worth pointing out that DeMHE serves as a preferable candidate for the problem considered in Chapter 3. In particular, we consider multiple soil profiles in a field. And it is found that several one-dimensional (1D) models that have negligible dynamic interactions can be used jointly to characterize the three-dimensional (3D) soil moisture dynamics in this circumstance. Therefore, distributed estimation is not a necessity due to the relatively weak interactions between two soil profiles, and decentralized estimation can be adopted so that fairly accurate estimates can be obtained while minimal information exchange between local agents can be achieved.

1.2 Thesis Outline and Contributions

The outline and contributions of the thesis is organized as follows:

In Chapter 2, an 1D Richards equation with spatially and temporally homogeneous parameters is considered for parameter and state estimation. First, the explicit finite difference (FD) model of Richards equation is developed. This is followed by the construction of the augmented system, which is achieved by augmenting parameters at the end of the state vector. The observability of the augmented system is tested using Popov-Belevitch-Hautus (PBH) observability theory, in order to identify the identifiable parameters. Then sensitivity analysis is used to choose the most important parameter set for estimation. The minimum number of sensors to ensure the identifiability of the parameter set is determined using the maximum multiplicity theory. Three common estimation schemes (EKF, EnKF and MHE) are applied on the 1D augmented model of Richards equation, in order to estimate the parameter set determined before, using only the minimum number of measurements. The estimation performance is compared and analyzed based on extensive simulations.

In Chapter 3, the estimation problem is extended to estimate the parameters and states of a 3D Richards equation with spatially heterogeneous and temporally homogeneous pa-

rameters. The steps to construct explicit 3D FD model are detailed and the effect of spatial discretization size on the numerical solution of 3D Richards equation is examined experimentally. The augmentation of the system and the determination of significant parameter set for estimation purpose follow the same ideas in the previous chapter. Subsystem decomposition scheme is discussed and the interaction between subsystems is qualitatively analyzed. DeMHE is proposed for parameter and state estimation and its performance is assessed based on simulations.

Chapter 2

Simultaneous Parameter and State Estimation of 1D Infiltration Processes

In this chapter, we focus on simultaneous parameter and state estimation of 1D infiltration process using MHE, EKF, and EnKF. We assume the parameters of the system are spatially and temporally homogeneous. We first introduce the investigated system and the formulation of the mathematical model in Section 2.1.1. The formulations of the estimation methods, MHE, EKF, and EnKF are introduced in Section 2.2. Section 2.3 includes the methods to determine the identifiable and significant parameters and the minimum number of sensors required to estimate parameters. Section 2.4 shows the simulation setup, results of determination of significant parameters and minimum number of sensors, and the results of MHE estimation compared with EKF and EnKF, followed by concluding remarks in Section 2.5. Chapter 2 is a revised version of [52].

2.1 Preliminaries

2.1.1 System Description and Problem Formulation

An agro-hydrological system describes the water movements between soil, crop and atmosphere. Figure 2.1 shows a schematic of an agro-hydrological system, which is a modified version from Reference [53]. The water movements usually involve water transportation within the soil, root water extraction, transpiration and evaporation from the soil and leaves to the air and precipitation including rain and irrigation.

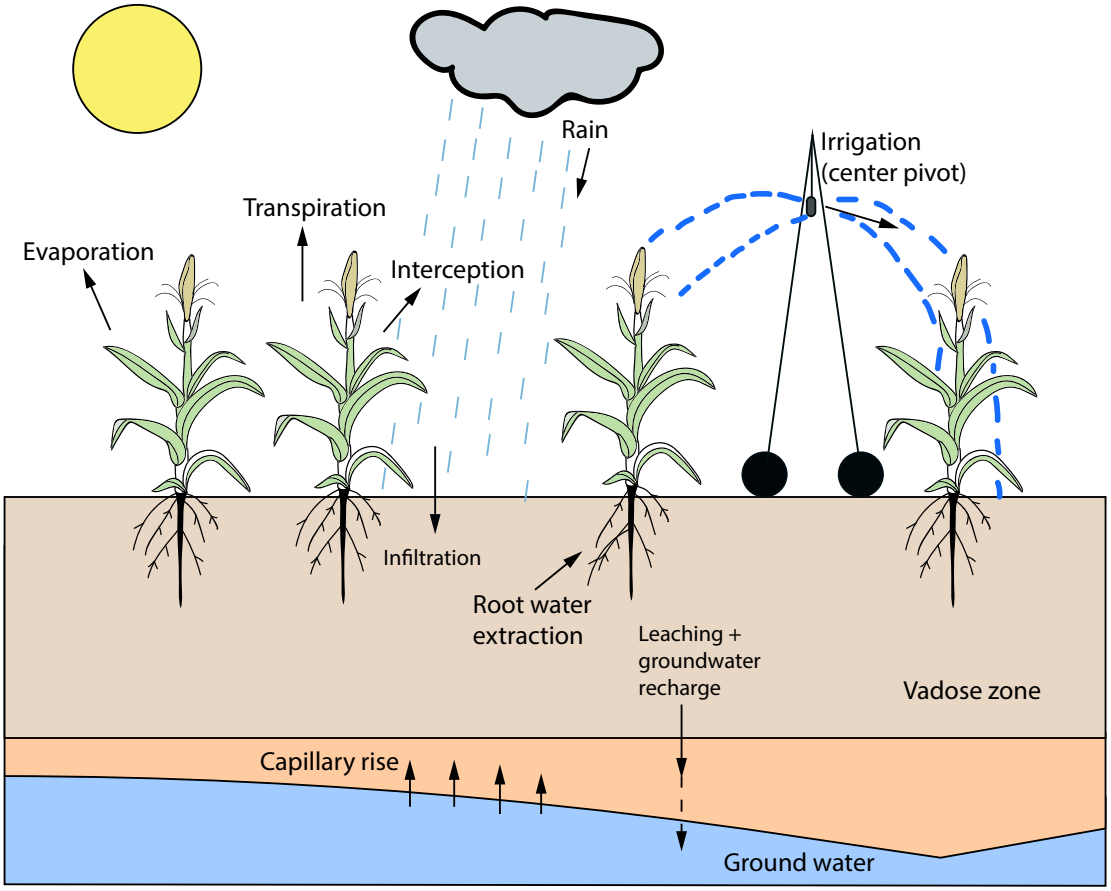

Figure 2.1: A schematic diagram of an agro-hydrological system.

In this work, we focus on soil that is above the water table (i.e., soil in the vadose zone). Within the vadose zone, the water movement is mainly driven by capillary and gravitational forces and the water dynamics can be modeled using Richards equation under the

assumptions: (1) soil properties are spatially homogeneous within the system; (2) irrigation is uniformly applied on the surface of the system; and (3) the horizontal water dynamics are much smaller than the vertical dynamics due to the gravity force and the horizontal water dynamics can be neglected. Then, the 1D Richards equation modeling the vertical water dynamics is shown below [54]:

$$c\left(h\right)\frac{\partial h}{\partial t}=\frac{\partial}{\partial z}\left[K\left(h\right)\left(\frac{\partial h}{\partial z}+1\right)\right] \tag{2.1}$$

In Equation (2.1), h (m) is the capillary potential in the unsaturated soil, $K(h)$ (m/s) and $c(h)$ (1/m) denote hydraulic conductivity and capillary capacity of the soil, respectively. Note that in Richards equation, the value 1 on the right-hand-side denotes the impact of gravitational force on water in the vertical (z) direction. The upward z direction is defined as the positive direction. The van Genuchten-Mualem soil hydraulic model $K(h)$ and $c(h)$, as functions of the capillary potential h, are shown as follows [10]:

$$K\left(h\right)=K_s\left[\left(1+\left(-\alpha h\right)^n\right)^{-\left(1-\frac{1}{n}\right)}\right]^{\frac{1}{2}}\left[1-\left[1-\left[\left(1+\left(-\alpha h\right)^n\right)^{-\left(1-\frac{1}{n}\right)}\right]^{\frac{n}{n-1}}\right]^{1-\frac{1}{n}}\right]^2 \tag{2.2}$$

$$c\left(h\right)=\left(\theta_s-\theta_r\right)\alpha n\left(1-\frac{1}{n}\right)\left(-\alpha h\right)^{n-1}\left[1+\left(-\alpha h\right)^n\right]^{-\left(2-\frac{1}{n}\right)} \tag{2.3}$$

where K_s (m/s), θ_s (m^3/m^3) and θ_r (m^3/m^3) are saturated hydraulic conductivity, saturated soil moisture and residual soil moisture, respectively. The van Genuchten-Mualem parameters α (1/m) and n characterize the properties of the soil, which are proportional to the inverse of the soil air entry pressure and of soil porosity, respectively. These two closed-form expressions are derived by van Genuchten based on his expression of soil-water retention curve and Mualem's open-form expression of hydraulic conductivity. Since Mualem's expression is not studied further, in this work, only van Genuchten's soil-water retention equation

is shown below [10]:

$$\theta(h) = (\theta_s - \theta_r)\left[\frac{1}{1+(-\alpha h)^n}\right]^{1-\frac{1}{n}} + \theta_r \tag{2.4}$$

where θ (m^3/m^3) denotes volumetric water content in soil.

The five parameters θ_s, θ_r, α, n and K_s determine the properties of a type of soil. With sufficient soil samples, θ_s, θ_r, α and n can be estimated by fitting the soil-water retention curve Equation (2.4) utilizing soil moisture and capillary potential data sets. Then K_s can be estimated by fitting hydraulic conductivity and capillary potential data sets into Equation (2.2). By using this approach, we can only get a snapshot of the soil properties at one time instant, however, soil properties do slowly change over time due to agricultural activities [55]. While the experiments can be repeated to get parameter estimates at different times, it is very time consuming and expensive, especially when the investigated field is large and has various soil types over the field. Therefore, online state and parameter estimation based on ease-to-access field measurements provides a favorable approach to estimate soil properties.

In this chapter, we study the estimation of soil properties based on real-time field measurements: capillary potential h.

2.1.2 Finite Difference Model Development

Richards equation is a nonlinear PDE with respect to both the temporal and spatial variables. Because of its complex structure, it is difficult to have a closed-form solution. Therefore a finite difference method is implemented to find a numerical approximation of its solution. Two-point forward difference scheme and two-point central difference scheme are used to approximate the derivatives with respect to the temporal and spatial variables, respectively:

$$\frac{\partial h_k(t)}{\partial t} = \frac{h_k(t+1) - h_k(t)}{\Delta t} \tag{2.5}$$

$$\frac{\partial}{\partial z}\left[K_k\left(h\left(t\right)\right)\left(\frac{\partial h_k\left(t\right)}{\partial z}+1\right)\right]=\frac{K_{k-\frac{1}{2}}\left(h\left(t\right)\right)\left(\frac{h_{k-1}(t)-h_k(t)}{\frac{1}{2}(\Delta z_{k-1}+\Delta z_k)}+1\right)-K_{k+\frac{1}{2}}\left(h\left(t\right)\right)\left(\frac{h_k(t)-h_{k+1}(t)}{\frac{1}{2}(\Delta z_k+\Delta z_{k+1})}+1\right)}{\Delta z_k} \tag{2.6}$$

where $t \in [0, N_t] \subset \mathbb{Z}$ and $k \in [1, N_x] \subset \mathbb{Z}$, representing time and position indices, respectively. N_t and N_x are the total number of time instants and total number of states, respectively. Δt denotes the forward time step and Δz_k represents thickness of compartment k. A schematic of the spatial discretization is shown in Figure 2.2. For illustration purpose, a column is discretized into 3 compartments ($k-1$, k and $k+1$). In each compartment, there is a state locating at its center. The hydraulic conductivity, for example, $K_{k-\frac{1}{2}}$, is linearized explicitly as $K_{k-\frac{1}{2}}(h) = K(\frac{h_{k-1}+h_k}{2})$.

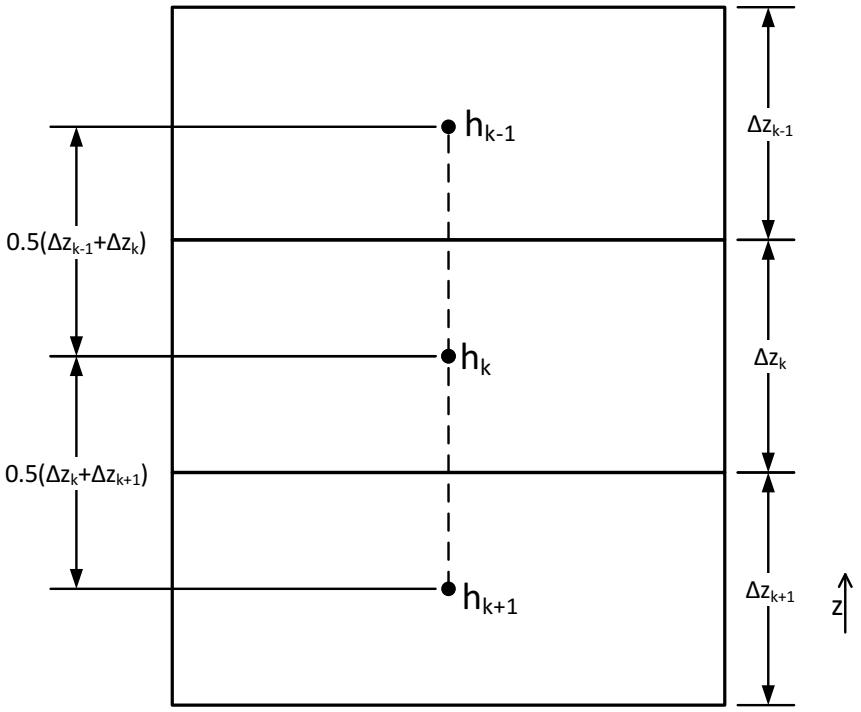

Figure 2.2: A schematic diagram of the spatial discretization.

The discrete-time finite difference model at node k and time instant $t+1$ can be obtained

by substituting Equations (2.5) and (2.6) into Equation (2.1) as follows:

$$h_k(t+1) = h_k(t) + \Delta t \frac{K_{k-\frac{1}{2}}(h(t)) \left(\frac{h_{k-1}(t)-h_k(t)}{\frac{1}{2}(\Delta z_{k-1}+\Delta z_k)} + 1 \right) - K_{k+\frac{1}{2}}(h(t)) \left(\frac{h_k(t)-h_{k+1}(t)}{\frac{1}{2}(\Delta z_k+\Delta z_{k+1})} + 1 \right)}{\Delta z_k c_k(h(t))} \tag{2.7}$$

where $c_k(h(t))$ is defined as $c(h_k(t))$.

The Neumann boundary condition is utilized to characterize the top and bottom boundaries of the system and are shown below, respectively:

$$\left. \frac{\partial h\,(t)}{\partial z} \right|_T = -1 - \frac{q_T(t)}{K\,(h\,(t))} \tag{2.8}$$

$$\left. \frac{\partial\,(h\,(t)+z)}{\partial z} \right|_B = 1 \tag{2.9}$$

where the subscripts T and B represent the top and bottom boundary conditions, respectively. The q_T (m/s) is the irrigation rate which is considered as the input of the system and free drainage boundary condition is applied at the bottom.

Before introducing estimation methods, for the sake of simplicity, we obtain the compact form of the model by combining N_x Equation (2.7) for all spatial nodes and the boundary conditions, Equations (2.8) and (2.9). It is shown below:

$$x\,(t+1) = F\,(x\,(t)\,, u\,(t)\,, p\,(t)) + \omega_x\,(t) \tag{2.10}$$

where $x(t) \in \mathbb{X} \subset \mathbb{R}^{N_x}$ represents the state vector containing N_x capillary pressure values for corresponding spatial nodes, at the defined time instant t. $p(t) \in \mathbb{P} \subset \mathbb{R}^{N_p}$, represents the parameter vector containing the parameters to be estimated. $u(t) \in \mathbb{U} \subset \mathbb{R}^{N_u}$, $\omega_x(t) \in \mathbb{W}_x \subset \mathbb{R}^{N_{\omega_x}}$ denote the input and the model disturbances, respectively.

The general output function, with the measurement noise taken into account, is shown below:

$$y\,(t) = G\,(x\,(t)\,, p\,(t)) + \nu\,(t) \tag{2.11}$$

where $y(t) \in \mathbb{Y} \subset \mathbb{R}^{N_y}$ and $\nu(t) \in \mathbb{V} \subset \mathbb{R}^{N_\nu}$ denote the measurement vector and measurement noise. If the volumetric soil moisture θ is measured by the soil moisture sensor, Equation (2.11) is the general form of Equation (2.4). On the other hand, if tensiometers are used to measure the water potential h in the soil, Equation (2.11) simply represents a matrix indicating which states are measured by the tensiometers.

Furthermore, in order to estimate the states and parameters simultaneously, the parameter vector is augmented at the end of the state vector and treated as a part of the augmented state vector, $x_a = [x,\ p]^T$. An estimation of the augmented state vector x_a brings the benefit to estimate the states and parameters at the same time. The augmented model can be constructed by augmenting Equation (2.10) with the following equation:

$$p\left(t+1\right) = p\left(t\right) + \omega_p\left(t\right) \tag{2.12}$$

where $\omega_p(t) \in \mathbb{W}_p \subset \mathbb{R}^{N_{\omega_p}}$. When the parameter vector p is assumed to be constant during the study, ω_p is equal to 0.

At last, the augmented model and output function used for simultaneous parameter and state estimation are shown below:

$$\begin{aligned} x_a\left(t+1\right) &= F_a\left(x_a\left(t\right), u\left(t\right)\right) + \omega_a\left(t\right) \\ y\left(t\right) &= G_a\left(x_a\left(t\right)\right) + \nu\left(t\right) \end{aligned} \tag{2.13}$$

where $x_a(t) \in \mathbb{X}_a \subset \mathbb{R}^{N_x+N_p}$, $\omega_a(t) \in \mathbb{W}_a \subset \mathbb{R}^{N_w+N_p}$ and the subscript a of $F(\cdot)$ and $G(\cdot)$ denotes the augmentation.

2.2 Estimation Methods

In this chapter, three common estimation schemes, MHE, EKF and EnKF are applied to the augmented model to estimate the states and parameters. The design of these methods

are detailed next.

2.2.1 Moving Horizon Estimation

MHE is an online optimization based estimation method [28]. The MHE optimization problem used in this work is formulated as follows:

$$\min_{\substack{\hat{x}_a(t-N),\cdots,\hat{x}_a(t),\\ \hat{\omega}_a(t-N),\cdots,\hat{\omega}_a(t-1)}} \|\hat{x}_a(t-N) - \bar{x}_a(t-N)\|^2_{P^{-1}} + \sum_{j=t-N}^{t-1} \|\hat{\omega}_a(j)\|^2_{Q^{-1}} + \sum_{j=t-N}^{t} \|\hat{\nu}(j)\|^2_{R^{-1}} \quad (2.14a)$$

$$\text{s.t. } \hat{x}_a(j+1) = F_a(\hat{x}_a(j), u(j)) + \hat{\omega}_a(j), \quad j \in [t-N, t-1] \subset \mathbb{Z} \quad (2.14b)$$

$$\hat{\nu}(j) = y(j) - G_a(\hat{x}_a(j)), \quad j \in [t-N, t] \subset \mathbb{Z} \quad (2.14c)$$

$$\bar{x}_a(t-N) = \hat{x}_a(t-N|t-N) \quad (2.14d)$$

$$\hat{x}_a(j) \in \mathbb{X}_a, \ \hat{\nu}(j) \in \mathbb{V}, \quad j \in [t-N, t] \subset \mathbb{Z} \quad (2.14e)$$

$$\hat{\omega}_a(j) \in \mathbb{W}_a, \quad j \in [t-N, t-1] \subset \mathbb{Z} \quad (2.14f)$$

In the MHE optimization, the objective is to minimize the distance between the predicted and observed measurements which is measured by the term $\|\hat{\nu}\|^2_{R^{-1}}$ as shown in Equation (2.14a), where the term $\hat{\nu}$ is defined in Equation (2.14c). The caret sign $\hat{}$ indicates that the variable is estimated. The model uncertainty or the process disturbance is taken into account and represented by $\|\hat{\omega}_a\|^2_{Q^{-1}}$, where the term $\hat{\omega}_a$ is defined in Equation (2.14b). The arrival cost, $\|\hat{x}_a - \bar{x}_a\|^2_{P^{-1}}$ summarizes the information from the initial state of the model up to the beginning of the estimation window of the MHE. N denotes the length of the estimation window. After each optimization, only the last estimated state within the estimation window is used. $\hat{x}_a$ and $\hat{\omega}_a$ within the moving window are the decision variables of the optimization problem. The term $\bar{x}_a$ follows the definition of Equation (2.14d). $\hat{x}_a(t-N|t-N)$ represents the estimated state $\hat{x}_a$ at time instant $t-N$, which is estimated at time instant $t-N$. Matrices P, Q, R are positive definite matrices and they are the covariance matrices

of state uncertainty, process noise ω_a and measurement noise ν, respectively. In addition, MHE takes into account constraints on the states, parameters and model uncertainties as expressed in Equations (2.14e) and (2.14f).

2.2.2 Extended Kalman Filter

EKF is a common method used for state estimation of nonlinear systems based on successively linearizing the nonlinear system. It can be divided into two steps, which are prediction and update steps. The prediction step predicts the state $\dot{x}$a and the state covariance matrix P. When a new measurement is available, the Kalman gain K is calculated first and then $\dot{x}$a and P are updated. The detailed steps are shown below:

1. Prediction step

   (a) State prediction:

   $$\hat{x}_a(t|t-1) = F_a(\hat{x}_a(t-1|t-1), u(t-1))$$

   The model disturbance are not propagated as the states and parameters. Instead, it is explicitly included in the state covariance prediction.

   (b) State covariance prediction:

   $$P(t|t-1) = A_a(t)P(t-1|t-1)A_a(t)^T + Q$$

   where $A_a(t) = \frac{\partial F_a}{\partial x_a}\Big|_{\hat{x}_a(t-1|t-1)}$ and Q is the covariance matrix of the model disturbance ω_a.

2. Update step

(a) Kalman gain calculation:

$$K(t) = P(t|t-1)C_a(t)^T[C_a(t)P(t|t-1)C_a(t)^T + R]^{-1}$$

where $C_a(t) = \frac{\partial G_a}{\partial x_a}\Big|_{\hat{x}_a(t|t-1)}$ and R is the covariance matrix of the measurement noise ν.

(b) State update:

$$\hat{x}_a(t|t) = \hat{x}_a(t|t-1) + K(t)\left(y(t) - G_a(\hat{x}_a(t|t-1))\right)$$

The augmented state and parameter vector x_a is updated when a new measurements $y(t)$ is available.

(c) State covariance update:

$$P(t|t) = \left(I - K(t)C_a(t)\right)P(t|t-1)$$

State covariance matrix P is updated. I is the identity matrix with dimension $N_x + N_p$.

2.2.3 Ensemble Kalman Filter

The EnKF is a method developed by Evensen [56] based on Monte Carlo method. An ensemble of trajectories of the system is generated based on the priori probability distribution of the case. A practical implementation scheme which estimated the probability distribution based on the information embedded within ensembles, instead of propagation of the state covariance matrix P, is discussed in Reference [57]. Unlike EKF, it directly utilizes the nonlinear model Equation (2.13), which does not require frequent model linearization. In addition, the model disturbance and measurement noise are taken into account at the same

time as the states and parameters propagate. It starts with generating the ensembles, then follows with the two steps as the same as in EKF.

1. Initialization step

   (a) Generating ensembles:

$$\hat{x}_a^m(0|0) \sim \mathcal{N}(x_a(0), P(0)), \quad m \in [1, M] \subset \mathbb{Z}$$

   where an ensemble containing M initial states $\hat{x}_a^m(0|0)$, $m = 1, \ldots, M$, is generated and m is the index of the ensemble. The ensemble follows the multivariate normal distribution with mean, $x_a(0)$ and covariance matrix of the initial state, $P(0)$.

2. Prediction step

   (a) State prediction:

$$\hat{x}_a^m(t|t-1) = F_a(\hat{x}_a^m(t-1|t-1), u(t-1)) + \omega_a^m(t-1), \quad m \in [1, M] \subset \mathbb{Z}$$

   where $\omega_a^m(t-1) \sim \mathcal{N}(0, Q)$. Just like generating the ensemble of $\hat{x}_a^m$, a normally distributed set of ω_a^m are generated with the mean 0 and the covariance matrix Q. Overall M trajectories propagate, with model disturbance explicitly considered.

3. Update step

   (a) Kalman gain calculation:

$$K(t) = P_{xy}(t|t-1)P_{yy}(t|t-1)^{-1}$$

   where

$$P_{xy}(t|t-1) = \frac{1}{M-1}\sum_{m=1}^{M}[(\hat{x}_a^m(t|t-1) - \bar{x}_a(t|t-1))(\hat{y}^m(t|t-1) - \bar{y}(t|t-1))]$$

$$P_{yy}(t|t-1) = \frac{1}{M-1}\sum_{m=1}^{M}[\hat{y}^m(t|t-1) - \bar{y}(t|t-1)]^2$$

$\bar{x}_a(t|t-1) = \frac{1}{M}\sum_{m=1}^{M} \hat{x}_a^m(t|t-1)$ and

$\bar{y}(t|t-1) = \frac{1}{M}\sum_{m=1}^{M} \hat{y}^m(t|t-1)$.

P_{xy} is the cross-covariance matrix of the state and measurement vectors and P_{yy} is the auto-covariance matrix of the measurement vector. The mean of the state or measurement vector is calculated based on the corresponding ensembles.

(b) State update:

$$\hat{x}_a^m(t|t) = \hat{x}_a^m(t|t-1) + K(t)\left[y(t) + \nu^m(t) - G_a(\hat{x}_a^m(t|t-1))\right], \quad m \in [1, M] \subset \mathbb{Z}$$

where $\nu^m(t) \sim \mathcal{N}(0, R)$. All M state vectors are updated, when the new measurement $y(t)$ is available. The measurement uncertainty is taken into account by generating a normally distributed ensemble of measurement noises $\nu^m(t)$, which has mean 0 and covariance matrix R. At last, the estimated state $\hat{x}_a(t|t)$ is obtained as the mean of the corresponding ensembles $\hat{x}_a^m(t|t)$, $m = 1, \ldots, m$.

2.3 Proposed Procedure to Determine Significant Parameters and Number of Sensors

In reality, it is nearly impossible to measure all states and the parameters can not be determined easily. First, according to Reference [58], it states that the original system of Equation (2.10) is observable using limited number of measurements. That means the states can be recovered. However, for this work the augmented system of Equation (2.13) is studied. For this case, it is necessary to ensure that the parameters are also identifiable since they are estimated with the states simultaneously. The proposed procedure to check the identifiability of the parameters, to select appropriate parameters for estimation and to determine the minimum number of sensors is shown in Figure 2.3. The key steps are explained below.

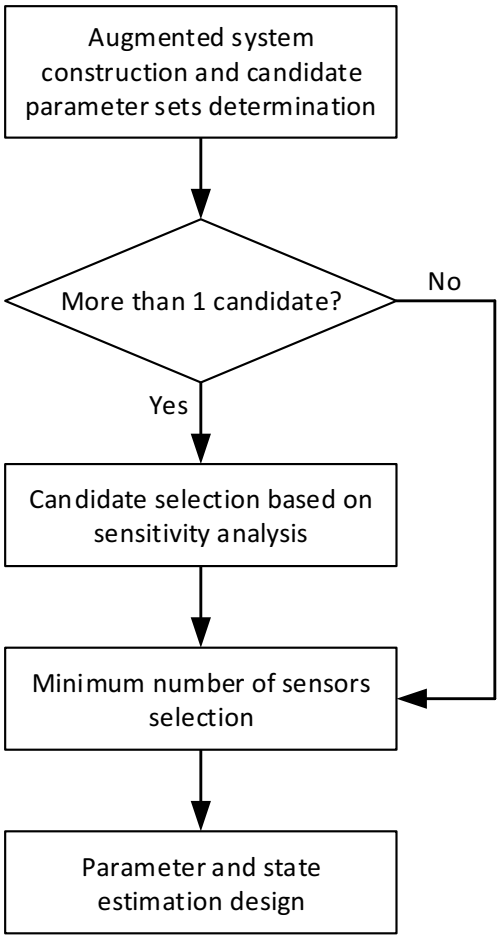

Figure 2.3: A flowchart of the procedure to determine the significant parameters and number of sensors.

2.3.1 Determine Candidate Parameter Sets for Estimation

After augmenting the original nonlinear system with the parameters, the entire system may not be observable. In order to determine which parameters can and should be estimated online, we resort to observability analysis [59]. In this step, we assume that all the soil moisture states are measured; that is, $y = x$. This ensures that the observability analysis results depend only on the parameters. If the augmented system is not observable, then the unobservability is caused by the augmentation of the parameters in the state vector.

When checking the observability of the augmented system, we start with the system with

all the parameters augmented. If the augmented system is not observable, then one of the parameters is removed from the augmented system. If there are N_p parameters, then there are N_p different ways to remove the one parameter. All these N_p cases are considered. If after removing one parameter and upon finding that the new augmented system is observable, we continue to the next step to determine which parameter set to estimate (described in the next subsection). If we can still not find an observable augmented system after removing one parameter, we continue to remove two parameters from the original augmented system. Again, all the possible cases should be considered. If we can still not find an observable system, we continue to remove three parameters from the original augmented system. This continues until we find at least a system that is observable.

When checking the observability, we propose to use the PBH observability theory. Other observability tests may also be used. Since the augmented system is a nonlinear system, it should be linearized before PBH can be applied. It is recommended that instead of linearizing the system at one point, it should be linearized at different point along typical operating trajectories as used in Reference [60].

Note that the observability analysis described in this step may generate more than one candidate parameter sets that can be estimated through augmentation of the original agro-hydrological system.

2.3.2 Sensitivity Analysis

If there is only one candidate parameter set from the previous step, we can continue with the candidate and move to the next subsection to find the minimum number of sensors. However, if there are more than one candidates, we need to determine which parameter set to choose. We propose to use sensitivity analysis to determine the importance of these parameters and pick the set containing the most important parameters for further analysis.

The sensitivity analysis measures how the outputs respond when there is a change in one parameter. The sensitivity matrix $S_y(t)$ shown below contains the information about,

at time instant t, how each output is affected by $x_a(0)$ which is constituted of the initial state $x(0)$ and the parameters p.

$$S_y(t) = \left[\begin{array}{cccc|ccc} \frac{\partial y_1}{\partial x_{a,1}(0)} & \frac{\partial y_1}{\partial x_{a,2}(0)} & \cdots & \frac{\partial y_1}{\partial x_{a,N_x}(0)} & \frac{\partial y_1}{\partial x_{a,N_x+1}(0)} & \cdots & \frac{\partial y_1}{\partial x_{a,N_x+N_p}(0)} \\ \frac{\partial y_2}{\partial x_{a,1}(0)} & \frac{\partial y_2}{\partial x_{a,2}(0)} & \cdots & \frac{\partial y_2}{\partial x_{a,N_x}(0)} & \frac{\partial y_2}{\partial x_{a,N_x+1}(0)} & \cdots & \frac{\partial y_2}{\partial x_{a,N_x+N_p}(0)} \\ \vdots & \vdots & \vdots & \vdots & \vdots & \vdots & \vdots \\ \frac{\partial y_{N_y}}{\partial x_{a,1}(0)} & \frac{\partial y_{N_y}}{\partial x_{a,2}(0)} & \cdots & \frac{\partial y_{N_y}}{\partial x_{a,N_x}(0)} & \frac{\partial y_{N_y}}{\partial x_{a,N_x+1}(0)} & \cdots & \frac{\partial y_{N_y}}{\partial x_{a,N_x+N_p}(0)} \end{array}\right]\Bigg|_t$$

The detailed steps to derive the sensitivity matrix is explained below and is inspired by Reference [61]. When performing this sensitivity analysis, we consider the augmented system of Equation (2.13) without considering the disturbance ω_a and ν but with $x_a(0)$ explicitly expressed as shown below:

$$\begin{aligned} x_a(t+1) &= F_a(x_a(t), u(t), x_a(0)) \\ y(t) &= G_a(x_a(t), x_a(0)) \end{aligned} \tag{2.15}$$

where $x_a(0)$ is considered as an independent variable.

The objective is to check how a change in the initial state x_0 and the parameters p affects the prediction error e, which comes from the difference between the predicted y and the observed measurements y_M. We can represent this as:

$$\frac{\partial e}{\partial x_a(0)} = \frac{\partial \left(y - y_M\right)}{\partial x_a(0)} = \frac{\partial y}{\partial x_a(0)} - \frac{\partial y_M}{\partial x_a(0)} \tag{2.16}$$

Because the observed measurement y_M is not affected by the initial state and parameters, the above expression is simplified as below:

$$\frac{\partial e}{\partial x_a(0)} = \frac{\partial y}{\partial x_a(0)} \tag{2.17}$$

Equation (2.17) can be derived by taking the partial derivative of Equation (2.15) with

respect to the augmented state vector $x_a(0)$. And the sensitivity equations with respect to $x_a(0)$ are shown below:

$$\begin{aligned}\frac{\partial x_a(t+1)}{\partial x_a(0)} &= \frac{\partial}{\partial x_a(0)} F_a(x_a(t), u(t), x_a(0)) \\ \frac{\partial y(t)}{\partial x_a(0)} &= \frac{\partial}{\partial x_a(0)} G_a(x_a(t), x_a(0))\end{aligned} \tag{2.18}$$

Because the intermediate variable $x_a(t)$ depends on the independent variable $x_a(0)$ as well, the chain rule is applied on the right hand sides of Equation (2.18) and we can further get that

$$\begin{aligned}\frac{\partial x_a(t+1)}{\partial x_a(0)} &= \frac{\partial F_a}{\partial x_a(t)} \cdot \frac{\partial x_a(t)}{\partial x_a(0)} + \frac{\partial F_a}{\partial x_a(0)} \\ \frac{\partial y(t)}{\partial x_a(0)} &= \frac{\partial G_a}{\partial x_a(t)} \cdot \frac{\partial x_a(t)}{\partial x_a(0)} + \frac{\partial G_a}{\partial x_a(0)}\end{aligned} \tag{2.19}$$

By defining $S_{x_a}(t) = \frac{\partial x_a(t)}{\partial x_a(0)}$ and $S_y(t) = \frac{\partial y(t)}{\partial x_a(0)}$, the above equations can be converted to ordinary differential equations, which are shown below:

$$\begin{aligned}S_{x_a}(t+1) &= \frac{\partial F_a}{\partial x_a(t)} \cdot S_{x_a}(t) + \frac{\partial F_a}{\partial x_a(0)} \\ S_y(t) &= \frac{\partial G_a}{\partial x_a(t)} \cdot S_{x_a}(t) + \frac{\partial G_a}{\partial x_a(0)}\end{aligned} \tag{2.20}$$

Therefore, by giving the initial states of Equations (2.15) and (2.20) and solving them at the same time, the sensitivity matrix $S_y(t)$ can be obtained. $S_y(t)$ may be normalized to obtain the normalized sensitivity matrix S_N:

$$S_N(t) = \frac{\partial y(t)}{\partial x_a(0)} \cdot \frac{x_a(0)}{y(t)} \tag{2.21}$$

Once the sensitivity matrix is obtained, we can use it to determine the relative importance of different parameters. Specifically, we can exam the magnitudes of the elements in the sensitivity matrix. Each parameter corresponds to one column in the sensitivity matrix. We can use, for example, the summation of the absolute values of the elements of each column

to compare the relative importance of parameters. A bigger value implies a more important parameter in terms of its impact on the outputs. Among all the candidate parameter sets, we keep the parameter set with the highest sensitivity values.

2.3.3 Minimum Number of Sensors

After the parameter set to be estimated is determined, the original system is augmented with the parameters, as illustrated in Reference [58], we can use the maximum multiplicity theory [62] to determine the minimum number of sensors required to ensure the observability of the entire system. Then, state estimation techniques can be used to estimate the states and parameters simultaneously.

2.4 Simulation Results and Discussion

2.4.1 System Description

In this work, a total length (L) of 67 cm loam soil column is investigated, which is shown in Figure 2.4. The soil column is equally partitioned into 32 compartments. Correspondingly, Richards equation is spatially discretized into 32 states (N_x) in the z direction, with each state centered at the corresponding compartment. At the surface of the soil, the irrigation, q_T, is performed at the rate of 2.50 cm/day, from 12:00 PM to 4:00 PM daily. At the bottom, the free drainage boundary condition is used, which means the gradient between the last state and the state at the bottom boundary is 0. The soil column has the homogeneous initial condition ($x(0)$) of -0.514 m capillary pressure head and the parameters of the soil are shown in Table 2.1 [63]. The code is written in Python and the simulations are carried out on a computer with Intel i5 CPU, 8.00 GB RAM.

Table 2.1: The initial condition and parameters of the investigated loam soil column.

	$x(0)$ (m)	K_s (m/s)	θ_s (m^3/m^3)	θ_r (m^3/m^3)	α (1/m)	n
Loam	-0.514	2.89×10^{-6}	0.430	0.0780	3.60	1.56

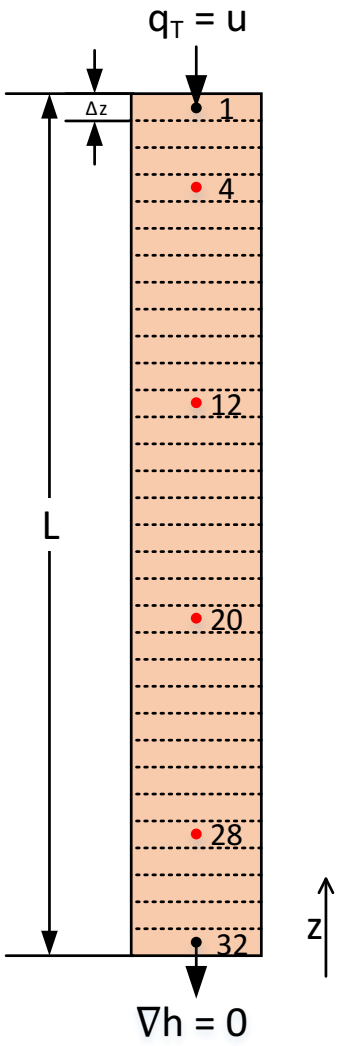

Figure 2.4: A schematic diagram of the investigated loam soil column.

2.4.2 Determination of Significant Parameters and Number of Sensors

The augmented system (Equation (2.13)) is utilized to achieve simultaneous parameter and state estimation. First without knowing the observability of the augmented system, all 5 parameters (K_s, θ_s, θ_r, α and n) are augmented; that is, $N_p = 5$. In addition, all 32 states are assumed to be measured. A 10-day state trajectory, without considering the process and measurement noise, is used in the rest of the subsection for selecting appropriate parameters for estimation and determining the minimum number of sensors. It is assumed that the measurements are available every 1 h.

Following the procedure as discussed in Section 2.3.1, we apply the PBH observability test on the augmented system to check the identifiability of the parameters. The test is conducted every sampling time, which requires the system to be linearized accordingly. According to the results, the augmented system is not observable. This implies that it is impossible to identify the 5 parameters simultaneously. In order to look for an observable system, parameters are removed from the augmented system. We start with removing only 1 of the parameters and this results in 5 different augmented systems with each one augmented with 4 parameters. Then, the observability of the 5 augmented systems is checked. It was found that 2 of the 5 systems are observable. In these two systems, either θ_s or θ_r is removed. Since observable systems are found, we proceed to the next step to determine the final parameter set.

To determine which parameter set to use, the significance of θ_s and θ_r is compared based on the sensitivity analysis described in Section 2.3.2. Sensitivity analysis is conducted based on the original augmented system with all the parameters. The initial state of Equation (2.20) is an identity matrix of size N_x+N_p. By comparing the summation of the absolute values of the elements of each column of the normalized sensitivity matrices S_N, it can be found that the summation corresponding to the column $\frac{\partial y_k}{\partial \theta_s}$ (82,674) is much bigger than the one for $\frac{\partial y_k}{\partial \theta_r}$ (14,997). Based on this, θ_s is considered as a more important parameter because it has more impact on the output than θ_r. Therefore, the parameter set containing θ_r is

Table 2.2: True values of initial states and parameters of the process and the initial guesses used in filters and estimator.

	$x(0)$ (m)	K_s (m/s)	θ_s (m^3/m^3)	α (1/m)	n	θ_r (m^3/m^3)
Loam (true value)	-0.514	2.89×10^{-6}	0.430	3.60	1.56	0.0780
Initial guess	-0.617	3.18×10^{-6}	0.387	3.24	1.72	0.0780

removed and the final parameter set will be used in the remaining analysis is $\{K_s, \theta_s, \alpha, n\}$.

In the above analysis, it was assumed that all the states (soil moisture) are measured for the purpose of determining the parameters for estimation. When the set of parameters is determined, we remove this assumption to determine the minimum number of sensors (measurements) needed to ensure the observability of the augmented system with 4 parameters. Following the method described in Section 2.3.3, the maximum multiplicity method is conducted, and it can be found that the minimum number of sensors is 4.

2.4.3 Simultaneous Parameter and State Estimation

According to the minimum number of sensors found above, it is assumed that 4 tensiometers (N_y) are installed. Specifically, we assume that these sensors are installed at 7.30 cm, 24.1 cm, 40.8 cm and 57.6 cm below the surface, which measure the 4th, 12th, 20th and 28th states, respectively. In the simulations, the actual parameter values used are shown in Table 2.1 and they are assumed to be constant within the investigated temporal domain. Process noise and measurement noise (ω_x and ν) are considered in the simulations and they have zero mean and standard deviations 3×10^{-6} m and 8×10^{-3} m, respectively.

In the design of the state and parameter filters (EKF, EnKF) and estimator (MHE), the model augmented with 4 parameters (K_s, θ_s, α and n) is used. The initial guesses of the initial states and parameters in the filters and estimator are listed in Table 2.2 and compared with those used in the actual system.

For the EKF and EnKF, the weighting matrices Q and R are designed as the auto-covariance matrices of ω_x and ν with the standard deviations mentioned before. However, the diagonal elements of Q corresponding to augmented parameters are 0, because the pa-

Table 2.3: Lower and upper bounds used in MHE.

	$\hat{x}$ (m)	$\hat{K}_s$ (m/s)	$\hat{\theta}_s$ (m^3/m^3)	$\hat{\alpha}$ (1/m)	$\hat{n}$	$\hat{\omega}_x$	$\hat{\omega}_p$
Lower bounds	-1.00	2.31×10^{-6}	0.344	2.88	1.25	$-\infty$	0.00
Upper bounds	-1.00×10^{-4}	3.47×10^{-6}	0.516	4.32	1.87	∞	0.00

rameters are assumed to be constant. In simulations, 10^{-20} is used to approximate the value 0 and to ensure the positive definiteness of the matrix. The diagonal elements of P corresponding to the states are configured as the square of 3×10^{-3} and those of parameters are configured as the square of 3×10^{-2}. For the designed EnKF, 100 ensembles are used.

For the design of MHE, the estimation window size is selected to be 8 h. The weighting matrices P, Q, and R retain the same ratio with respect to those used in EKF and EnKF but with a much bigger magnitude to ensure the numerical stability of the associated optimization problem. In addition, the P matrix is constant for all the optimizations. The constraints of the states, parameters and the model uncertainty are listed in Table 2.3. The upper and lower bounds of the term $\hat{\omega}_p$ are 0 because the parameters are constant.

In the following simulations, the root mean square error (RMSE) will be used to evaluate the performance of the MHE, EKF and EnKF. The estimation performance in terms of the states and parameters are evaluated separately. Their equations are shown below:

$$RMSE_x(t) = \sqrt{\frac{\sum_{k=1}^{N_x}(\hat{x}_k(t) - x_k(t))^2}{N_x}} \tag{2.22}$$

$$RMSE_p(t) = \sqrt{\frac{\sum_{k=1}^{N_p}(\hat{p}_k(t) - p_k(t))^2}{N_p}} \tag{2.23}$$

First, we performed simulations assuming that the parameter θ_r (which is not estimated) is known and is the same as the value used in the actual system. Figures 2.5 and 2.6 show some representative estimated states and all the parameters using MHE, EKF and EnKF, which are also compared with their true values. Figure 2.5 shows the state trajectories of the top node and a few middle nodes and one bottom node. From the figure, it can be seen that the top node has more dynamics because it takes time for irrigated water to pass from the

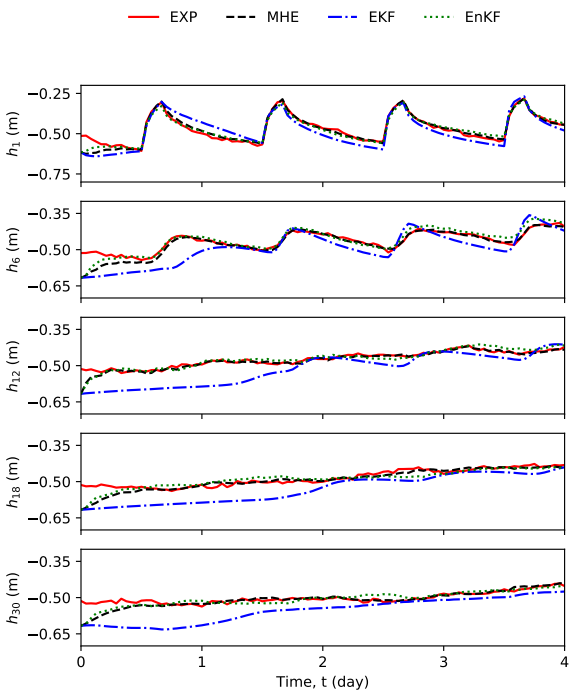

Figure 2.5: Selected trajectories of the process states and estimated states using MHE, EKF and EnKF.

upper part and to the lower part. In terms of state estimation performance, from Figure 2.5, it can be seen that MHE and EnKF give very much more accurate state estimates than the EKF. Note that from Figure 2.5, it can also be seen that the estimates of the 12th state (h_{12}) converge faster than the other estimates. This is because it is a sensor node. In terms of parameter estimation, Figure 2.6 shows the results. From the figure, it can be seen that only MHE is capable of estimating the parameters, whereas those estimated by EKF and EnKF diverge from their true values. This may be because of the constraints used in MHE. These constraints provide more useful information to MHE in addition to the measurements.

The trajectories of the performance indices $RMSE_x$ and $RMSE_p$ associated with the MHE, EnKF and EKF are shown in Figure 2.7. These trajectories further confirm that the MHE and EnKF have better performance than EKF in estimation of the states and the MHE outperforms both EnKF and EKF in parameter estimation.

In the previous set of simulations, the parameter θ_r is assumed to be accurately known

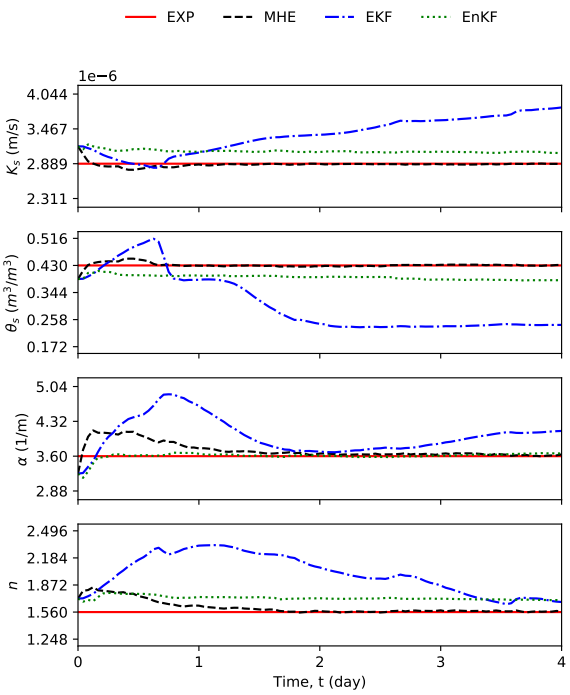

Figure 2.6: Trajectories of estimated parameters using MHE, EKF and EnKF, compared with their actual values.

and is used in the MHE, EnKF and EKF. However, this assumption may not hold in practice. In this set of simulations, we study how an inaccurate θ_r may affect the state and parameter estimation performance. In this set of simulations, the value of θ_r used in the MHE, EnKF and EKF is assumed to be 10% off from the actual value. The tuning parameters used in the filters and estimator are the same as the ones used in the previous simulations. In this case, the EnKF and EKF cannot give accurate parameter estimates as in the previous case, either. The MHE is still the only estimation method that can give good parameter estimates. Table 2.4 summarizes the estimated parameters using the MHE in the two sets of simulations. The reported estimated values are the mean estimated values after the estimates have converged. According to the results, a 10% difference of θ_r does not affect the estimation results of other parameters when MHE is used. This verifies that the removal of θ_r has a minor impact on the overall state and parameter estimation performance. This further implies that the proposed method in parameter selection is applicable.

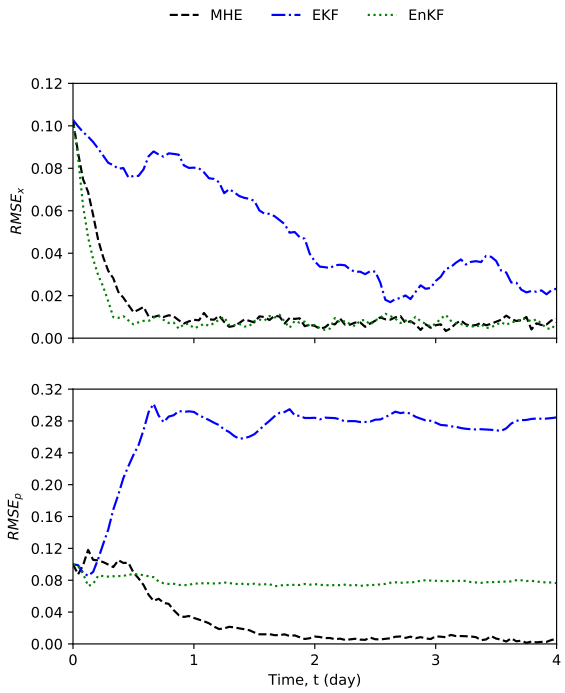

Figure 2.7: Trajectories of RMSE measuring the estimation performance of MHE, EKF, and EnKF.

Table 2.4: Comparison of estimated parameters using MHE with their true values, when θ_r is assumed to be accurate and 10% off.

Cases	θ_r (m^3/m^3)	$\hat{K}_s$ (m/s)	$\hat{\theta}_s$ (m^3/m^3)	$\hat{\alpha}$ ($1/m$)	$\hat{n}$
θ_r (true value)	0.0780	2.89×10^{-6}	0.430	3.60	1.56
$\hat{\theta}_r$ ($= \theta_r$)	0.0780	2.89×10^{-6}	0.430	3.60	1.56
$\hat{\theta}_r$ ($= 90\%\theta_r$)	0.0702	2.89×10^{-6}	0.430	3.60	1.56

In this work, the spatial heterogeneity in soil properties is not considered. When parameter heterogeneity presents, a 3D Richards equation is needed to describe the water dynamics. The studied MHE algorithm can be extended to handle heterogeneous parameters in a straightforward manner. It is expected that the weighting matrices should be tuned taking into account the spatial heterogeneity. Also, a system with different soil types may be decomposed into a few subsystems with each subsystem having the same type of soil and distributed or decentralized estimation may be used accordingly. MHE may still be used in the design of the subsystem estimators.

2.4.4 Effects of Simulation Parameters

In this subsection, we further study the performance of MHE in terms of number of measurements and size of estimation window of MHE.

2.4.4.1 Effects of Number of Measurements

First, we study the effects of number of measurements on the estimation performance of MHE. In addition to the case with 4 measurements, we also consider cases with 8 and 12 measurements. Figure 2.8 shows how the two performance indices $RMSE_x$ and $RMSE_p$ evolve over time. From the top plot, it can be seen that the more sensors are used, the faster state estimates converge. This is because the sensors are directly measuring the states. When there are more sensors, it implies that we have more information of the states. For the parameter, there is no obvious difference between the convergence speeds with different number of measurements. Comparing the convergence speed between the state estimates and parameter estimates, the state estimates converge much faster within one day while the parameter estimates take longer time to converge (about 2 days). Overall, from this set of simulations, it can be concluded that 4 sensors are sufficient to estimate all states and parameters accurately.

2.4.4.2 Effects of MHE Estimation Window Size

The effects of the size of the estimation window of MHE on estimation performance are also studied assuming that there are 4 measurements. Figure 2.9 shows how the two performance indices $RMSE_x$ and $RMSE_p$ evolve over time with different estimation window sizes. From the figure, it can be seen that from both plots that a window size of 8 is sufficient and further increase of the estimation window size does not bring significant performance improvement.

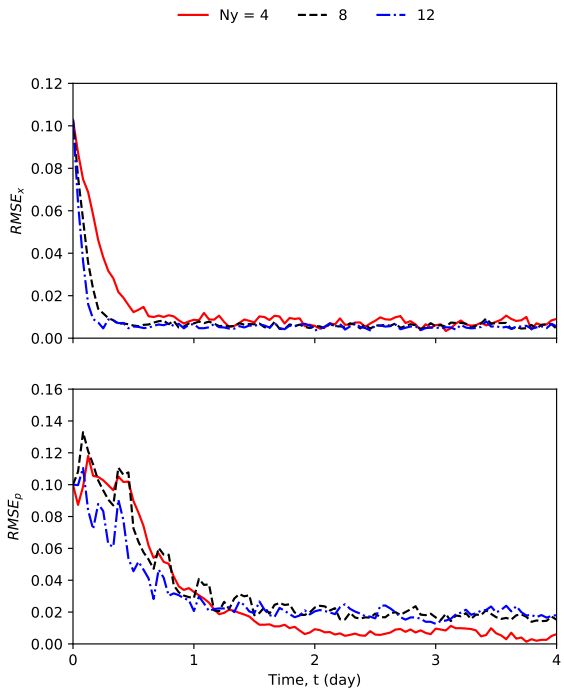

Figure 2.8: Trajectories of RMSE measuring the error between actual model and estimated states and parameters of MHE using 4, 8 and 12 measurements.

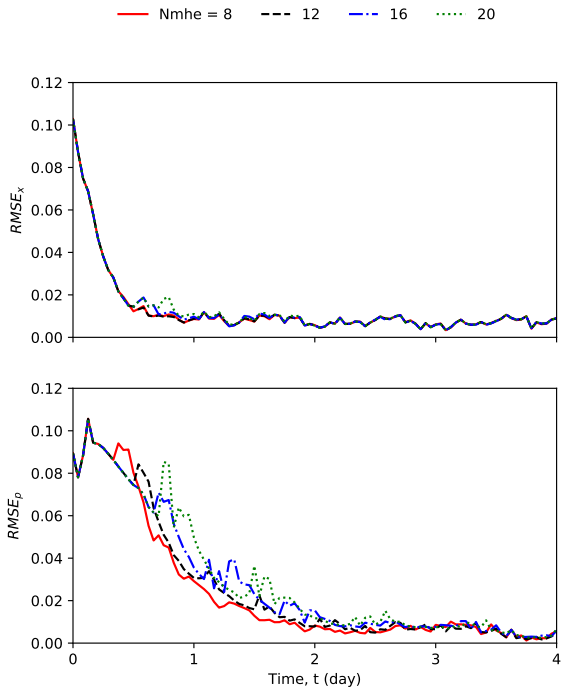

Figure 2.9: Trajectories of RMSE measuring the error between actual model and estimated states and parameters of MHE with window sizes of 8, 12, 16 and 20.

2.5 Summary

In this chapter, we have investigated simultaneous state and parameter estimation using MHE, EKF, and EnKF applied to an infiltration system. First, a procedure was proposed to find the appropriate parameter set for estimation based on the observability of the augmented system and the sensitivity of the outputs to the parameters. It was found that only four out of five parameters (hydraulic conductivity, saturated soil moisture, and van Genuchten-Mualem parameters) can be considered in simultaneous state and parameter estimation. The less important parameter (residual soil moistures) was not considered in parameter estimation. After determining the parameter set for estimation, by using the maximum multiplicity theory, the minimum number of sensors to ensure the identifiability of parameters was four. Simulation results showed that the MHE has an overall the best parameter and state estimation performance due to the inclusion of state and parameter constraints in the estimation. It was also found that the uncertainty in the residual soil moisture (which was not estimated) does not affect the overall estimation performance too much. The effects of number of measurements and estimation window size of the MHE were also studied through simulations. It was found that four measurements and a window size of eight for MHE are sufficient to provide accurate parameter and state estimates.

Chapter 3

Simultaneous Parameter and State Estimation of 3D Infiltration Processes

In this chapter, we study a simultaneous parameter and state estimation of 3D infiltration processes, which have spatially heterogeneous and temporally homogeneous parameters, using DeMHE. First, the investigated 3D system, the construction of the numerical model and augmented model are introduced in Section 3.1. The subsystem decomposition guidelines and the formulation of DeMHE are presented in Section 3.2. The simulation results and discussion are shown in Section 3.3 including the simulation setup, a study on spatial discretization size, observability test and DeMHE estimation results. Section 3.4 summarizes the work covered in this chapter.

3.1 Preliminaries

3.1.1 System Description and Problem Formulation

A piece of field may have complex terrains, such as hill, valley, etc. It may contain more than one type of soil at different locations, for example, loam, clay, sand, etc. These facts cause complicated horizontal water movements, which further affect the irrigation water-use efficiency. Due to the horizontal water movements, different areas have different soil moistures. Hence, if the movement can be captured, the closed-loop irrigation controller could irrigate the appropriate amount of water to different areas according to their soil moistures caused by the complicated terrains and various soil types. For example, the controller could irrigate more water at the top of the hill than the bottom, since runoff would happen and more water will be stored at the bottom. In another case, the sand has less capability to store water for the crops, hence, more water can be irrigated at this area to supply sufficient water to the crops.

In this chapter, in order to capture the dynamics of a field with multiple soil profiles, it is essential to introduce the 3D agro-hydrological system. A simplified field with multiple types of soil is studied under the following assumptions. First, the soil heterogeneity only presents in horizontal direction and the interface between two types of soil is vertical and flat. In other words, we assume that there is no mixture of different types of soil in the system. Second, for each type of soil, the irrigation is uniformly applied on the surface. If the surface of one type of soil is significantly large and the irrigation equipment cannot cover the whole surface at the same time, this soil can be decomposed into sections with each section has the uniform irrigation/input. Third, the surface of the field is assumed to be flat, therefore, the effect of terrains is not studied. A schematic of the 3D agro-hydrological system is shown in Figure 3.1.

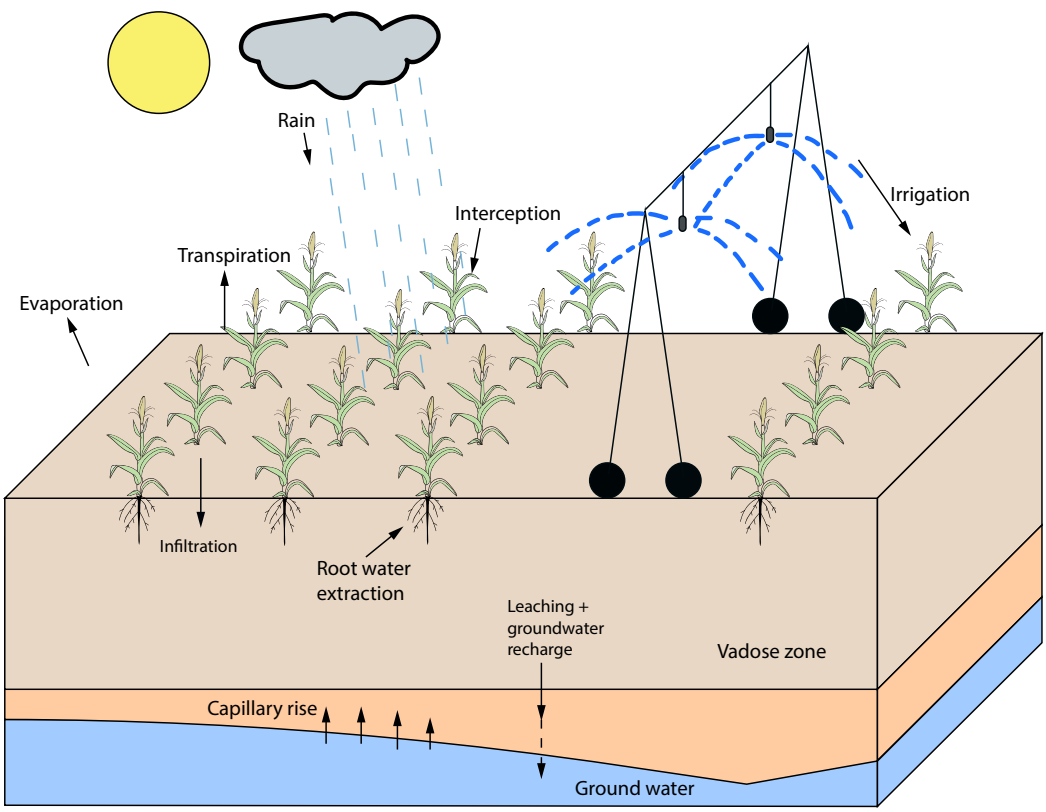

Figure 3.1: A schematic diagram of a 3D agro-hydrological system.

The governing equation, Richards equation, is extended into 3D and shown below:

$$c\left(h\right)\frac{\partial h}{\partial t}=\nabla\cdot\left[K\left(h\right)\nabla\left(h+z\right)\right] \tag{3.1}$$

where h (m) represents the capillary potential in the unsaturated soil, $K(h)$ (m/s) and $c(h)$ $(1/m)$ denote hydraulic conductivity and capillary capacity of the soil, respectively. The van Genuchten-Mualem soil hydraulic model $K(h)$ and $c(h)$ are utilized and shown as Equations (2.2) and (2.3), respectively. In van Genuchten-Mualem soil hydraulic model, the parameter set (K_s, θ_s, θ_r, α and n) determines the properties of the type of soil. When

Richards equation is used to describe the capillary potential of different types of soil, the values of parameter set are different. Note that in Richards equation, the term z on the right-hand-side denotes the impact of gravitational force on water in the vertical (z) direction. Compared with 1D Richards equation (Equation (2.1)), the vector differential operator (∇) in the 3D form summarizes the second derivatives of total pressure head with respect to x, y and z directions.

3.1.2 Finite Difference Model Development

The FD method is applied, in order to find the a numerical approximation of solution of (3.1). The procedure to construct the 3D FD model is detailed below.

First, the vector differential operation (∇) is carried out, which results in a less compact form:

$$c\left(h\right)\frac{\partial h}{\partial t}=\frac{\partial}{\partial x}\left(K(h)\frac{\partial h}{\partial x}\right)+\frac{\partial}{\partial y}\left(K(h)\frac{\partial h}{\partial y}\right)+\frac{\partial}{\partial z}\left[K(h)\left(\frac{\partial h}{\partial z}+1\right)\right] \tag{3.2}$$

Comparing to 1D Richards equation (Equation (2.1)), the right-hand side is the summation of three terms, which are the second derivatives of total pressure head in x, y, and z directions. The first and second terms govern the water movements in x and y directions, respectively. Because the gravity force is only applied on the water movement in the vertical (z) direction, $+z$ or $+1$ term does not present in the first and second terms.

The FD method, strictly speaking, two-point central difference scheme and two-point forward difference scheme are used to approximate the derivatives with respect to spatial and temporal domains, respectively. As shown below, Equations (3.3a), (3.3b), and (3.3c) show the approximations of the derivative terms with respect to x, y, and z directions.

Equation (3.3d) explains how the derivative in terms of time is approximated.

$$\begin{aligned}\left.\frac{\partial}{\partial x}\left(K(h(t))\frac{\partial h(t)}{\partial x}\right)\right|_{i,j,k} =& \frac{1}{\Delta x_i} \\ & \cdot\left[K_{i-\frac{1}{2},j,k}\left(h\left(t\right)\right)\left(\frac{h_{i-1,j,k}\left(t\right)-h_{i,j,k}\left(t\right)}{\frac{1}{2}(\Delta x_{i-1}+\Delta x_i)}\right)\right. \\ & \left.-K_{i+\frac{1}{2},j,k}\left(h\left(t\right)\right)\left(\frac{h_{i,j,k}\left(t\right)-h_{i+1,j,k}\left(t\right)}{\frac{1}{2}(\Delta x_i+\Delta x_{i+1})}\right)\right] \end{aligned} \tag{3.3a}$$

$$\begin{aligned}\left.\frac{\partial}{\partial y}\left(K(h(t))\frac{\partial h(t)}{\partial y}\right)\right|_{i,j,k} =& \frac{1}{\Delta y_j} \\ & \cdot\left[K_{i,j-\frac{1}{2},k}\left(h\left(t\right)\right)\left(\frac{h_{i,j-1,k}\left(t\right)-h_{i,j,k}\left(t\right)}{\frac{1}{2}(\Delta y_{j-1}+\Delta y_j)}\right)\right. \\ & \left.-K_{i,j+\frac{1}{2},k}\left(h\left(t\right)\right)\left(\frac{h_{i,j,k}\left(t\right)-h_{i,j+1,k}\left(t\right)}{\frac{1}{2}(\Delta y_j+\Delta y_{j+1})}\right)\right] \end{aligned} \tag{3.3b}$$

$$\begin{aligned}\left.\frac{\partial}{\partial z}\left[K(h(t))\left(\frac{\partial h(t)}{\partial z}+1\right)\right]\right|_{i,j,k} =& \frac{1}{\Delta z_k} \\ & \cdot\left[K_{i,j,k-\frac{1}{2}}\left(h\left(t\right)\right)\left(\frac{h_{i,j,k-1}\left(t\right)-h_{i,j,k}\left(t\right)}{\frac{1}{2}(\Delta z_{k-1}+\Delta z_k)}+1\right)\right. \\ & \left.-K_{i,j,k+\frac{1}{2}}\left(h\left(t\right)\right)\left(\frac{h_{i,j,k}\left(t\right)-h_{i,j,k+1}\left(t\right)}{\frac{1}{2}(\Delta z_k+\Delta z_{k+1})}+1\right)\right] \end{aligned} \tag{3.3c}$$

$$\left.\frac{\partial h\left(t\right)}{\partial t}\right|_{i,j,k} = \frac{h_{i,j,k}\left(t+1\right)-h_{i,j,k}\left(t\right)}{\Delta t} \tag{3.3d}$$

Note that in (3.3a) - (3.3d), the spatial index is represented by i, j, k and the temporal index is denoted by t. Specifically, $i \in [1, N_{x,x}] \subset \mathbb{Z}$, $j \in [1, N_{x,y}] \subset \mathbb{Z}$, and $k \in [1, N_{x,z}] \subset \mathbb{Z}$, where $N_{x,x}$, $N_{x,y}$, and $N_{x,z}$ denote the number of compartments in x, y, and z directions. $t \in [0, N_t] \subset \mathbb{Z}$ where N_t denotes the number of time instants. Δt denotes the temporal step size. Δx_i, Δy_j, and Δz_k represent the length (L_x), width (L_y), and depth (L_z) of the compartment, respectively. If the investigated spatial domain is discretized uniformly in each direction, Δx, Δy, and Δz are sufficient.

The hydraulic conductivity is explicitly linearized, for example,

$$K_{i-\frac{1}{2},j,k}(h) = K\left(\frac{h_{i-1,j,k}+h_{i,j,k}}{2}\right)$$

$$K_{i,j-\frac{1}{2},k}(h) = K\left(\frac{h_{i,j-1,k} + h_{i,j,k}}{2}\right)$$

$$K_{i,j,k+\frac{1}{2}}(h) = K\left(\frac{h_{i,j,k} + h_{i,j,k+1}}{2}\right)$$

The FD model, which calculates the capillary pressure head at the position i, j, k and the time instant $t+1$, is obtained by substituting Equations (3.3a) - (3.3d) into Equation (3.2). It is shown below:

$$\begin{aligned}
h_{i,j,k}(t+1) = h_{i,j,k}(t) + \frac{\Delta t}{c_{i,j,k}(h(t))} \\
\cdot \Bigg\{ \frac{1}{\Delta x_i} \Bigg[K_{i-\frac{1}{2},j,k}\left(h\left(t\right)\right) \left(\frac{h_{i-1,j,k}\left(t\right) - h_{i,j,k}\left(t\right)}{\frac{1}{2}(\Delta x_{i-1} + \Delta x_i)} \right) \\
- K_{i+\frac{1}{2},j,k}\left(h\left(t\right)\right) \left(\frac{h_{i,j,k}\left(t\right) - h_{i+1,j,k}\left(t\right)}{\frac{1}{2}(\Delta x_i + \Delta x_{i+1})} \right) \Bigg] \\
+ \frac{1}{\Delta y_j} \Bigg[K_{i,j-\frac{1}{2},k}\left(h\left(t\right)\right) \left(\frac{h_{i,j-1,k}\left(t\right) - h_{i,j,k}\left(t\right)}{\frac{1}{2}(\Delta y_{j-1} + \Delta y_j)} \right) \\
- K_{i,j+\frac{1}{2},k}\left(h\left(t\right)\right) \left(\frac{h_{i,j,k}\left(t\right) - h_{i,j+1,k}\left(t\right)}{\frac{1}{2}(\Delta y_j + \Delta y_{j+1})} \right) \Bigg] \\
+ \frac{1}{\Delta z_k} \Bigg[K_{i,j,k-\frac{1}{2}}\left(h\left(t\right)\right) \left(\frac{h_{i,j,k-1}\left(t\right) - h_{i,j,k}\left(t\right)}{\frac{1}{2}(\Delta z_{k-1} + \Delta z_k)} + 1 \right) \\
- K_{i,j,k+\frac{1}{2}}\left(h\left(t\right)\right) \left(\frac{h_{i,j,k}\left(t\right) - h_{i,j,k+1}\left(t\right)}{\frac{1}{2}(\Delta z_k + \Delta z_{k+1})} + 1 \right) \Bigg] \Bigg\}
\end{aligned} \tag{3.4}$$

where $c_{i,j,k}(h) = c(h_{i,j,k})$.

The Neumann boundary condition is used to characterize the top, bottom, left, right,

front, and back boundaries, which are shown below respectively:

$$\left.\frac{\partial h\left(t\right)}{\partial z}\right|_{i,j,0} = -1 - \frac{q_{i,j,0}(t)}{K\left(h\left(t\right)\right)} \tag{3.5a}$$

$$\left.\frac{\partial h\left(t\right)}{\partial z}\right|_{i,j,(N_{x,z}+1)} = -1 - \frac{q_{i,j,(N_{x,z}+1)}\left(t\right)}{K\left(h\left(t\right)\right)} \tag{3.5b}$$

$$\left.\frac{\partial h\left(t\right)}{\partial x}\right|_{0,j,k} = -\frac{q_{0,j,k}\left(t\right)}{K\left(h\left(t\right)\right)} \tag{3.5c}$$

$$\left.\frac{\partial h\left(t\right)}{\partial x}\right|_{(N_{x,x}+1),j,k} = -\frac{q_{(N_{x,x}+1),j,k}\left(t\right)}{K\left(h\left(t\right)\right)} \tag{3.5d}$$

$$\left.\frac{\partial h\left(t\right)}{\partial y}\right|_{i,0,k} = -\frac{q_{i,0,k}\left(t\right)}{K\left(h\left(t\right)\right)} \tag{3.5e}$$

$$\left.\frac{\partial h\left(t\right)}{\partial y}\right|_{i,(N_{x,y}+1),k} = -\frac{q_{i,(N_{x,y}+1),k}\left(t\right)}{K\left(h\left(t\right)\right)} \tag{3.5f}$$

In the above equations, if either of i, j or k equals to zero, it mean the boundary is either of left, front or top boundary, respectively. On the other hand, if it equals to either of $N_{x,x}+1$, $N_{x,y}+1$ or $N_{x,z}+1$, the boundary is either of right, back, or bottom boundary. The variable q (m/s) denotes the water flow rate, in particular, $q_{i,j,0}$ represents the irrigation rate supplied at the surface point i, j. It is considered as the input of the system. By following the standard 3D Cartesian coordinate system, when the water flows in the same direction of one of positive axes, the flow rate is defined as a positive value. On the contrary, the flow rate has a negative value when the water flows in the opposite direction. The incorporation of flux based boundary conditions into Richards equation is shown below with top boundary as an example.

By rearranging (3.5a), the irrigation rate can be represented as the following:

$$-q_{i,j,0}(t) = K(h(t))\left(\left.\frac{\partial h\left(t\right)}{\partial z}\right|_{i,j,0} + 1\right) \tag{3.6}$$

Since only unsaturated case is considered in this work, it is not necessary to calculate the value of the capillary pressure head at the top boundary ($h_{i,j,0}$), when calculating the

capillary pressure head at the top layer ($h_{i,j,1}$). Instead, the term in (3.4), which is shown below, can be substituted by Equation (3.6).

$$K_{i,j,\frac{1}{2}}\left(h\left(t\right)\right)\left(\frac{h_{i,j,0}\left(t\right)-h_{i,j,1}\left(t\right)}{\Delta z_0}+1\right)$$

Then $h_{i,j,1}$ is calculated by directly using the irrigation rate, $q_{i,j,0}$, instead of $h_{i,j,0}$.

3.1.3 Augmented Model Development

A compact form describing a 3D Richards equation can be obtained by combining Equations (3.4), (3.5b) - (3.5f), and (3.6) of all nodes, which is represented as below:

$$\begin{aligned} x(t+1) &= F(x(t),u(t),p(t))+\omega_x(t) \\ y(t) &= Cx(t)+\nu(t) \end{aligned} \tag{3.7}$$

where $x(t)\subset\mathbb{R}^{N_x}$ is the state vector, $u(t)\subset\mathbb{R}^{N_u}$ is the input vector, $p(t)\subset\mathbb{R}^{N_p}$ denotes the parameter vector, $\omega_x(t)\subset\mathbb{R}^{N_{\omega_x}}$ represents the system disturbance, $y(t)\subset\mathbb{R}^{N_y}$ is the system output vector, and $\nu(t)\subset\mathbb{R}^{N_\nu}$ denotes the measurement noise. The state is the capillary pressure head and the total number (N_x) of the states is the product of $N_{x,x}$, $N_{x,y}$ and $N_{x,z}$. The size of the parameter vector (N_p) depends on the types of soil presented in the system considered. Because a system with more than 1 type of soil is studied in this chapter, the value of N_p is greater than that of N_p in Chapter 2. The output is obtained by directly measuring some of the states.

The augmented model is constructed by following the same idea explained in the previous chapter, which is shown below:

$$\begin{aligned} x_a(t+1) &= F_a(x_a(t),u(t))+\omega_a(t) \\ y(t) &= C_a x_a(t)+\nu(t) \end{aligned} \tag{3.8}$$

where the subscript a denotes the augmentation, $x_a(t) \subset \mathbb{R}^{N_{x_a}}$ is the augmented state vector, which is $x_a = [x, p]^T$. The augmented model disturbance is denoted as $\omega_a(t) \subset \mathbb{R}^{N_{w_a}}$.

3.2 Estimation Method

Based on the estimation performance of MHE, EKF and EnKF compared in Chapter 2, MHE outperforms the other two methods in terms of handling the constraints and preventing the estimates from diverging. Therefore, in this chapter, we also choose to use MHE to estimate the parameters and states of 3D Richards equation. In reality, a reasonable agricultural field covers the area more than thousands of square meters, and more than millions of states are required to model the system. A centralized MHE framework may fail to provide online estimates due to increasingly high computational load included by the optimization [33, 35]. Therefore, a decentralized or distributed estimation scheme needs to be developed in this chapter. First, the guidelines for subsystem decomposition are introduced in Subsection 3.2.1. Subsection 3.2.2 discusses the method to test the observability of the original system and subsystems. Then, an analysis to motivate the use of a decentralized framework is carried out in Subsection 3.2.3. At last, Subsection 3.2.4 presents the design of DeMHE.

3.2.1 Guidelines for Subsystem Decomposition

In the development of a decentralized/distributed estimation scheme, the first step is to decompose the entire process into smaller subsystems. For the 3D infiltration system, we rely on the following guidelines:

1. it is expected that the numbers of the states in the configured subsystems can be made similar, such that the computational and organizational complexity of the local estimators are not significantly different;

2. it is desirable if each subsystem only accounts for one soil type;

3. it is expected the initial values of the states involved in each subsystem are relatively similar;

4. it is expected the areas that are subject to different irrigation schedules are assigned to different subsystems;

5. it is expected each configured subsystem is assigned sufficient sensors such that the decentralized estimation problem is feasible;

6. it is important that the dynamic interaction between each two subsystems is made minimal.

By following the guidelines, each subsystem represents a relatively small 3D field, which contains only 1 type of soil and its irrigation is uniformly applied. It is favorable, at least from theoretical view, to use 3D Richards equation to develop state and parameter estimation algorithm. However, 3D discretization will lead to increasing number of states, which MHE may not be able to handle in an online fashion. It is possible to use, for example, the states at the center column of the subsystem to approximate the capillary potentials of different nodes within the same subsystem, because the states in the same horizontal layer may be similar with each other under the proposed decomposition guidelines. Hence, in each subsystem, only 1D Richards equation is utilized for modeling vertical water dynamics, which significantly reduces the computational demand for each decentralized/distributed estimator. The formulation of 1D decomposed subsystems is shown below:

$$\begin{aligned} x_a^n(t+1) &= F_a^n(x_a^n(t), q^t(t), u^n(t)) + \omega_a^n(t) \\ y^n(t) &= C_a^n x_a^n(t) + \nu^n(t) \end{aligned} \tag{3.9}$$

where the superscript $n \in [1, N_s] \subset \mathbb{Z}$ denotes the index of the subsystem. $x_a^n(t) \subset \mathbb{R}^{N_{x_a^n}}$ is the state vector for the subsystem n. The state vector contains the states and parameters of the soil presented in the subsystem n. $y^n(t) \subset \mathbb{R}^{N_{y^n}}$ is the n^{th} subsystem output vector,

which is only related to the states from the same subsystem. The subsystem disturbance and measurement noise are represented as $\omega_a^n(t) \subset \mathbb{R}^{N_{\omega_a^n}}$ and $\nu^n(t) \subset \mathbb{R}^{N_{\nu^n}}$.

Note that $q^n(t) \subset \mathbb{R}^{N_{q^n}}$ represents the information obtained from the neighboring subsystem, which is required by the subsystem n.

3.2.2 Observability Test

Before conducting the subsystem decomposition, it is essential to conduct an observability test on the original system (3.8) to ensure the system is observable [36]. In addition, after configuring the subsystems through decomposition, it is necessary to check the observability of subsystems (3.9). The method used to test the observability is proposed in Section 2.3. At the same time, the significant parameter set for estimation is selected and the minimum number of sensors required to ensure the observability of subsystems is determined. After subsystems pass the observability test, decentralized/distributed estimation can be designed and conducted.

3.2.3 Motivation of Decentralized Estimation

In this subsection, the significance of interaction between subsystems is studied, which further motivates the use of a decentralized framework.

First, according to the FD model of 3D Richards equation (Equation (3.4)), the state at the next time instant ($h_{i,j,k}(t+1)$) is dependent on itself and its adjacent states at the current time instant (t). The physical locations of these states are shown in Figure 3.2. The states $h_{i,j,k}$, $h_{i,j,k-1}$ and $h_{i,j,k+1}$ belong to the same subsystem, and $h_{i-1,j,k}$, $h_{i+1,j,k}$, $h_{i,j-1,k}$ and $h_{i,j+1,k}$ belong to the neighbouring subsystems. Next, let us take a detailed analysis of the following term on the right-hand side of (3.4)

$$\frac{1}{\Delta x_i}\left[K_{i-\frac{1}{2},j,k}\left(h\left(t\right)\right)\left(\frac{h_{i-1,j,k}\left(t\right)-h_{i,j,k}\left(t\right)}{\frac{1}{2}(\Delta x_{i-1}+\Delta x_i)}\right)-K_{i+\frac{1}{2},j,k}\left(h\left(t\right)\right)\left(\frac{h_{i,j,k}\left(t\right)-h_{i+1,j,k}\left(t\right)}{\frac{1}{2}(\Delta x_i+\Delta x_{i+1})}\right)\right].$$

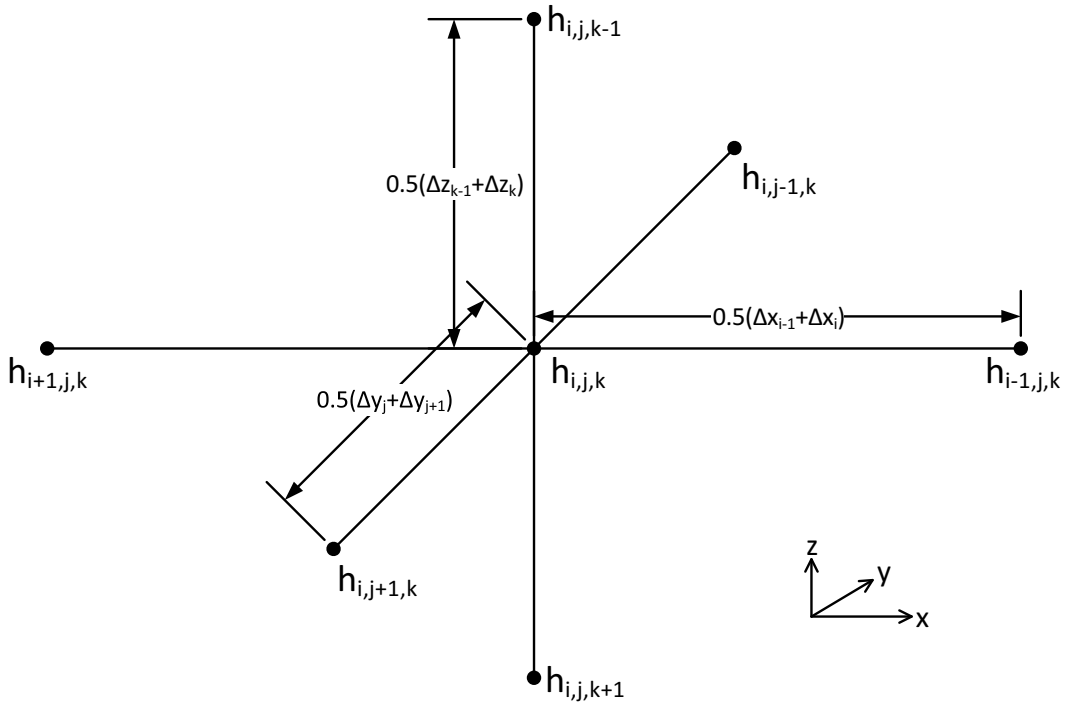

Figure 3.2: A diagram illustrating spatial relation between center state and neighboring states.

If the discretization in x direction is equally spaced, it can be further simplified into the following:

$$\frac{K_{i-\frac{1}{2},j,k}\left(h\left(t\right)\right)\left[h_{i-1,j,k}\left(t\right)-h_{i,j,k}\left(t\right)\right]-K_{i+\frac{1}{2},j,k}\left(h\left(t\right)\right)\left[h_{i,j,k}\left(t\right)-h_{i+1,j,k}\left(t\right)\right]}{\left(\Delta x\right)^{2}} \tag{3.10}$$

This term quantitatively measures how the neighboring states in x direction ($x_{i-1,j,k}$ and $x_{i+1,j,k}$) contribute to the propagation of $x_{i,j,k}$. In the same way, the following two terms quantify how neighboring states in y and z directions affect the propagation of $x_{i,j,k}$, respectively:

$$\frac{K_{i,j-\frac{1}{2},k}\left(h\left(t\right)\right)\left[h_{i,j-1,k}\left(t\right)-h_{i,j,k}\left(t\right)\right]-K_{i,j+\frac{1}{2},k}\left(h\left(t\right)\right)\left[h_{i,j,k}\left(t\right)-h_{i,j+1,k}\left(t\right)\right]}{\left(\Delta y\right)^{2}} \tag{3.11}$$

$$\frac{K_{i,j,k-\frac{1}{2}}\left(h\left(t\right)\right)\left[h_{i,j,k-1}\left(t\right)-h_{i,j,k}\left(t\right)+1\right]-K_{i,j,k+\frac{1}{2}}\left(h\left(t\right)\right)\left[h_{i,j,k}\left(t\right)-h_{i,j,k+1}\left(t\right)+1\right]}{\left(\Delta z\right)^{2}} \tag{3.12}$$

According to Equation (3.4), the summation of the above three terms contributes to the propagation of $x_{i,j,k}$. If there is a term which is significantly greater than others, it will affect more on the propagation. As mentioned before, Δx and Δy represent the distance between subsystems. They can be the value with the unit in meters and Δz may have the unit in centimeters, for example, Δx and Δy are equal to 10 m and Δz is equal to 1 cm. Then, the denominator of (3.12) is 10^6 times smaller than those of (3.10) and (3.11). Because the seven states shown in Figure 3.2 have the values in the similar magnitudes, the numerators of the above three terms are in the relatively similar magnitudes. Hence, the term (3.12) is around 10^6 times greater than terms (3.10) and (3.11), which implies that the contribution of the states in z direction ($x_{i,j,k-1}$ and $x_{i,j,k+1}$) to the propagation of $x_{i,j,k}$ is significantly bigger than those of states in x and y directions.

In other words, the horizontal interactions between the states are notably smaller, as compared to the vertical interactions between the states. In this study, because the horizontal interaction between the proposed subsystems is notably small, it can be neglected when designing the estimation scheme, such that decentralized MHE serves a good candidate solution.

3.2.4 Decentralized Moving Horizon Estimation Design

After the subsystem decomposition scheme is finalized, DeMHE is designed for the subsystems. The schematic diagram of DeMHE is shown in Figure 3.3. At the bottom section of the diagram, the system is decomposed into subsystems based on the type of soil. The arrows between the subsystems mean that there is information exchange between the neighboring subsystems. For example, if the subsystem 2 represents the soil column which is on the right hand side of the soil column governed by subsystem 1, the information $x_{a,2}$ denotes the states and parameters information required by the subsystem 2. The information is

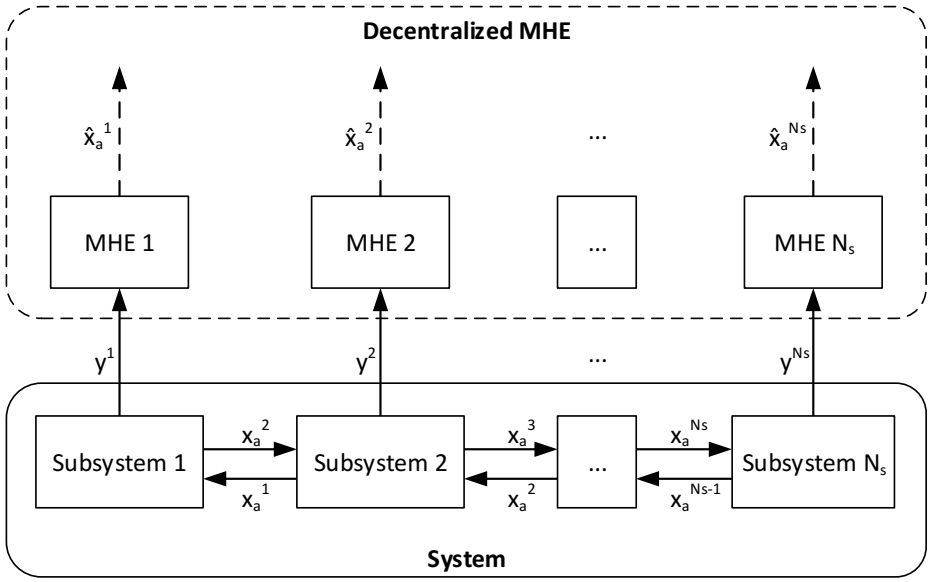

Figure 3.3: A schematic diagram of the proposed decentralized parameter and state estimation scheme.

from the right surface of the subsystem 1, which is considered as the left boundary of the subsystem 2. Similarly, $x_{a,1}$ is used by the subsystem 1 as the right boundary, which comes from the left surface of the subsystem 2. At every sampling time, the measurements from the subsystems are measured and sent to the corresponding estimators. The estimator will only utilize the measurements from the corresponding subsystem and not from other subsystems. Each estimator is isolated with each other in DeMHE. Therefore, at the top of the schematic diagram, there is not arrows or information exchange between the estimators. The model in each estimator, which is used to describe the corresponding subsystem, is also isolated. However, the model does require boundary conditions information which are available in other models. An assumption needs to be made on models' boundary conditions, and in this study, the left, right, front, and back boundary conditions of models used in estimators are assumed to be zero capillary potential gradient.

The mathematical formulation of the DeMHE describing the above scheme is shown

below:

$$\min_{\substack{\hat{x}_a^n(t-N^n),\cdots,\hat{x}_a^n(t),\\ \hat{\omega}_a^n(t-N^n),\cdots,\hat{\omega}_a^n(t-1)}} \|\hat{x}_a^n(t-N^n)-\bar{x}_a^n(t-N^n)\|^2_{(P^n)^{-1}}+\sum_{l=t-N^n}^{t-1}\|\hat{\omega}_a^n(l)\|^2_{(Q^n)^{-1}}+\sum_{l=t-N^n}^{t}\|\hat{\nu}^n(l)\|^2_{(R^n)^{-1}} \tag{3.13a}$$

$$\text{s.t. } \hat{x}_a^n(l+1)=F_a^n(\hat{x}_a^n(l),u^n(l))+\hat{\omega}_a^n(l),\quad l\in[t-N^n,t-1]\subset\mathbb{Z} \tag{3.13b}$$

$$\hat{\nu}^n(l)=y^n(l)-C_a^n\hat{x}_a^n(l),\quad l\in[t-N^n,t]\subset\mathbb{Z} \tag{3.13c}$$

$$\hat{x}_a^n(l)\in\mathbb{X}_a^n,\ \hat{\nu}^n(l)\in\mathbb{V}^n,\quad l\in[t-N^n,t]\subset\mathbb{Z} \tag{3.13d}$$

$$\hat{\omega}_a^n(l)\in\mathbb{W}_a^n,\quad l\in[t-N^n,t-1]\subset\mathbb{Z} \tag{3.13e}$$

where n denotes the index of the estimator. N^n is the estimation window size of the estimator n. The variables $\hat{x}_a^n$, $\hat{\omega}_a^n$, and $\hat{\nu}^n$ are the estimates of x_a^n, ω_a^n, and ν^n within the estimation window of the subsystem n. The penalty matrices P^n, Q^n, and R^n in the cost function (3.13a) are the covariance matrices of the subsystem's state uncertainty, model disturbance, and measurement noise. For different subsystems with different soil types, the design of the penalty matrices for each corresponding MHE could be different while the algorithms of MHE are the same. Overall, (3.13b) and (3.13c) are the subsystem model constraints, with information exchange term is dropped from (3.13b). The constraints of the subsystem state, disturbance, and measurement noise are denoted as $\mathbb{X}_a^n$, $\mathbb{W}_a^n$, and $\mathbb{V}^n$, which are shown in (3.13d) and (3.13e).

3.3 Simulation Results and Discussion

3.3.1 System Description

In this chapter, a field with 20 m (L_x) in x direction, 10 m (L_y) in y direction and total depth (L_z) of 67 cm is investigated, which is shown in Figure 3.4. The soil type is loam on the left half of the field and is sandy clay loam (SCL) on the right half. The parameters of

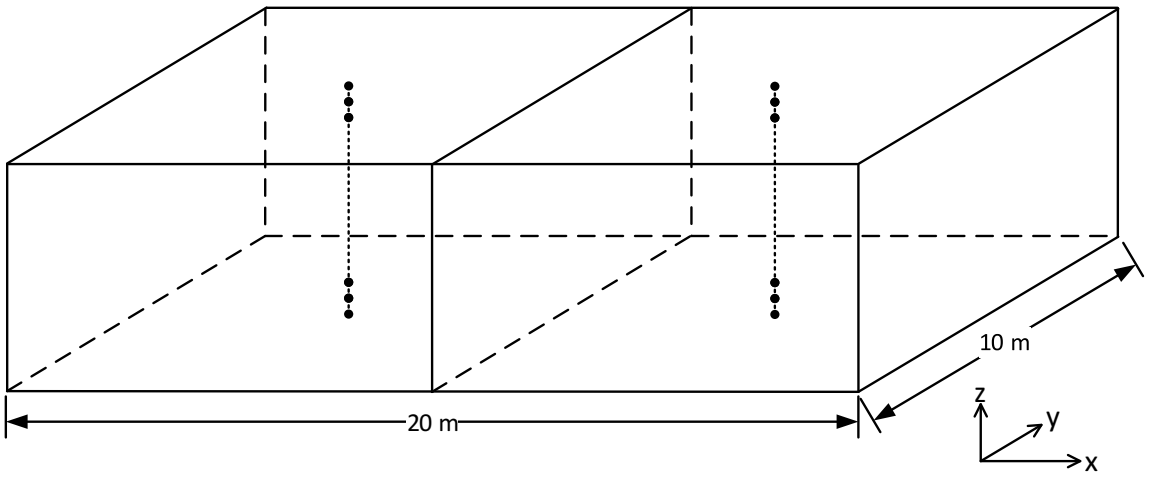

Figure 3.4: A schematic diagram of the investigated field.

Table 3.1: The parameters of the investigated 3D field.

	K_s (m/s)	θ_s (m^3/m^3)	θ_r (m^3/m^3)	α (1/m)	n
Loam	2.89×10^{-6}	0.430	0.0780	3.60	1.56
Sandy clay loam	3.64×10^{-6}	0.390	0.100	5.90	1.48

soils are shown in Table 3.1 [63]. In order to construct the FD model, the field is equally partitioned into 500 compartments in x direction, 250 compartments in y direction, and 32 compartments in z direction. Correspondingly, Richards equation is spatially discretized into 500 ($N_{x,x}$), 250 ($N_{x,y}$), and 32 states ($N_{x,z}$) in the x, y, and z directions, respectively. Each state is centered at the corresponding compartment, instead of at the vertices of the compartment. In the figure, the column of black solid dots represents the states of the compartments which are at the center column of each soil. The code is written in Python and the simulations are carried out on a computer with Intel i5 CPU, 8.00 GB RAM.

3.3.2 Observability Test on Original System

As described in Subsection 3.2.2, it is necessary to ensure the observability of the original system before decomposition. The system contains two different types of soil, loam and sandy clay loam. There will be 10 parameters in the augmented system and the result of

determination of significant parameters obtained in Chapter 2 cannot be accepted. The observability of the augmented system needs to be checked again to ensure the identifiability of the parameters. The method proposed in Section 2.3 is carried out again on the augmented 3D system (3.8) to check the identifiability of parameters, select the significant identifiable parameters, and determine the minimum number of sensors required to ensure the identifiability.

At the beginning, all 10 parameters (K_s, θ_s, θ_r, α, and n for loam and sandy clay loam) are augmented and all states are assumed to be measured. A 4-day deterministic state trajectory is simulated under the following setups: (1) on the surface of the soil, the irrigation (u) is performed at the rate of 2.50 cm/day, from 12:00 PM to 4:00 PM daily; (2) at the bottom, the free drainage boundary condition is applied, and (3) the field has the homogeneous initial condition ($x(0)$) of -0.514 m capillary pressure head. The simulation result is used in the rest of the subsection. The measurements are available every one hour.

Following the procedure discussed in Subsection 2.3.1, the PBH observability test is applied on the augmented system to check the identifiability of the parameters. The system needs to be linearized every time when the test is carried out, which is every sampling time. It shows that the augmented system is not observable when all 10 parameters are augmented, even all states are measured. In order to look for an observable system, parameters are removed from the augmented system. It starts with removing only one of the parameters and this results in 10 different augmented systems with each one augmented with nine parameters. It is found that none of systems are observable. Then, two parameters are removed from the system (3.8), which results in 45 different augmented systems. By checking their observability, it shows that there are four systems are observable. The parameters removed from these four candidates are listed in Table 3.2. Since observable systems are found, the final parameter set is determined in the next step.

Sensitivity analysis described in Subsection 2.3.2 is conducted based on the original augmented system with all the parameters augmented. By comparing 1-norm of each column of

Table 3.2: Observable systems and their removed parameters.

Candidate #	Parameters removed
1	θ_s of loam and θ_s of SCL
2	θ_r of loam and θ_r of SCL
3	θ_s of loam and θ_r of SCL
4	θ_r of loam and θ_s of SCL

the normalized sensitivity matrices S_N, it can be found that the 1-norm of the column $\frac{\partial y_i}{\partial \theta_s}$ of both loam (5050) and SCL (2.34) are bigger than 1-norm of $\frac{\partial y_i}{\partial \theta_r}$ of loam (916) and SCL (0.600), respectively. Based on this, θ_s of two soils are considered as the more important parameters because they have more impacts on the output than θ_r. It worth mentioning that even the 1-norm of $\frac{\partial y_i}{\partial \theta_s}$ of SCL (2.34) is much smaller than 1-norm of $\frac{\partial y_i}{\partial \theta_r}$ of loam (916), θ_r of loam is neglected in estimation problem. The reason is that if both θ_s and θ_r of loam are augmented in the system, the system becomes unobservable. Therefore, the parameter set (Candidate 2) excluding both θ_r is selected and the final parameter set used in the remaining analysis is $\{K_s, \theta_s, \alpha, n\}$ for both loam and sandy clay loam.

The identifiable and significant parameter set is determined based on the assumption that all states are measured. The minimum number of sensors (measurements) is determined, following the method described in Subsection 2.3.3. After the maximum multiplicity method is conducted, and it shows that the minimum number of sensors is 8 to ensure the observability of the augmented system with 8 parameters.

In conclusion, a system which is augmented with 8 parameters (K_s, θ_s, α, and n for both loam and sandy clay loam) is observable and it will be used in the next subsection for subsystem decomposition.

3.3.3 Subsystem Decomposition

By following the guidelines for subsystem decomposition in Subsection 3.2.1, it will result in 2 subsystems. Subsystem 1 contains 2 millions states representing the capillary potentials of loam on left half of the field, 4 parameters of loam augmented at the end of the state vector,

4 outputs measuring the loam, and 62500 inputs uniformly applied on the states in the top layers. Similarly, Subsystem 2 contains 2 millions states, 4 parameters treated as states, 4 outputs and 62500 inputs with respect to the SCL on the right half of the field. Because the soil property, initial state and input are uniform in each subsystem, it is reasonable to assume the state at the center column of the subsystem is able to represent the whole subsystem. Under this situation, each 3D subsystem is represented by an 1D model which contains 32 states, 4 augmented parameters, 4 outputs and 1 input. Figure 3.4 can be visualized as that the 3D system is discretized into 2 compartments in x direction and 1 compartment in y direction with a larger Δx and Δy; that is $\Delta x = 10$ m and $\Delta y = 10$ m. In addition, the 1D model is located at the center of the compartment.

In order to ensure the above assumptions are valid and reasonable, it is necessary to compare the numerical solutions of the models under two different discretization schemes. The first scheme is proposed in Subsection 3.3.1 and Δx and Δy equal to 4 cm. The second scheme is proposed in this subsection and Δx and Δy equal to 10 m. The model with Δx and Δy equal to 4 cm is called Model 1, and the one with 10 m is called Model 2. We assume that the numerical solution of Model 1 is able to represent the trajectories of the system accurately. Then this solution is compared with the solution of Model 2. If the percentage difference of the solutions of two models are acceptable, 10 m is considered as an acceptable discretization size in x and y directions, and the assumptions used for simplify subsystems are valid. Three scenarios are proposed and the setups are listed in Table 3.3. The numerical solutions of two models are compared in all three scenarios. Specifically, the setup of Scenario 1 is that at the surface of the soil, the irrigation (u) is performed at the rate of 2.50 cm/day, from 12:00 PM to 4:00 PM daily. At the bottom, the free drainage boundary condition is applied. The field has the homogeneous initial condition ($x(0)$) of -0.514 m capillary pressure head. Scenario 2 studies the impact of initial conditions. The left half of the field has the homogeneous initial condition of -0.514 m capillary pressure head and the right half has the homogeneous initial condition of -0.284 m. The top and

Table 3.3: The setups of scenarios studying effects of sizes of both Δx and Δy on numerical solution of 3D Richards equation.

	$x(0)$ (m)		u (cm/day)		Irrigation schedule	
	Loam	SCL	Loam	SCL	Loam	SCL
Scenario 1	-0.514	-0.514	2.5	2.5	12PM to 4PM	12PM to 4PM
Scenario 2	-0.514	-0.284	2.5	2.5	12PM to 4PM	12PM to 4PM
Scenario 3	-0.514	-0.514	2.5	2.5	12PM to 2PM	2PM to 4PM

bottom boundary conditions of this scenario is the same as the setup of Scenario 1. Scenario 3 studies the impact of inputs on the numerical solution. It has the same initial condition and bottom boundary condition as Scenario 1. However, the irrigation is performed at the rate of 2.5 cm/day, from 12:00 PM to 2:00 PM daily on the left half of the field and from 2:00 PM to 4:00 PM daily on the right half.

The following three figures, Figures 3.5, 3.6, and Figure 3.7, show the selected state trajectories comparing two models under Scenario 1, 2, and 3, respectively. Within each figure, the subplot on the left shows the trajectories of the loam and the subplot on the right shows the trajectories of sandy clay loam. Under each scenario, the trajectories of Model 2 is as almost the same as those of Model 1. Qualitatively speaking, the maximum percentage difference over the investigated time domain of Scenario 1, 2, and 3 is 0.01%, 0.03%, and 0.006%, respectively. Therefore, when both Δx and Δy equal to 10 m, it will not introduce numerical issues and the numerical solution of Model 2 represents the process accurately, under three proposed scenarios.

In conclusion, for a subsystem that contains only 1 type of soil, receives uniform irrigation and is initialized uniformly, the capillary potential at the center of the subsystem (black dots) is able to represent the capillary potentials at other locations in the same horizontal layer. Hence, it is reasonable to only use an 1D model to simulate the subsystem.

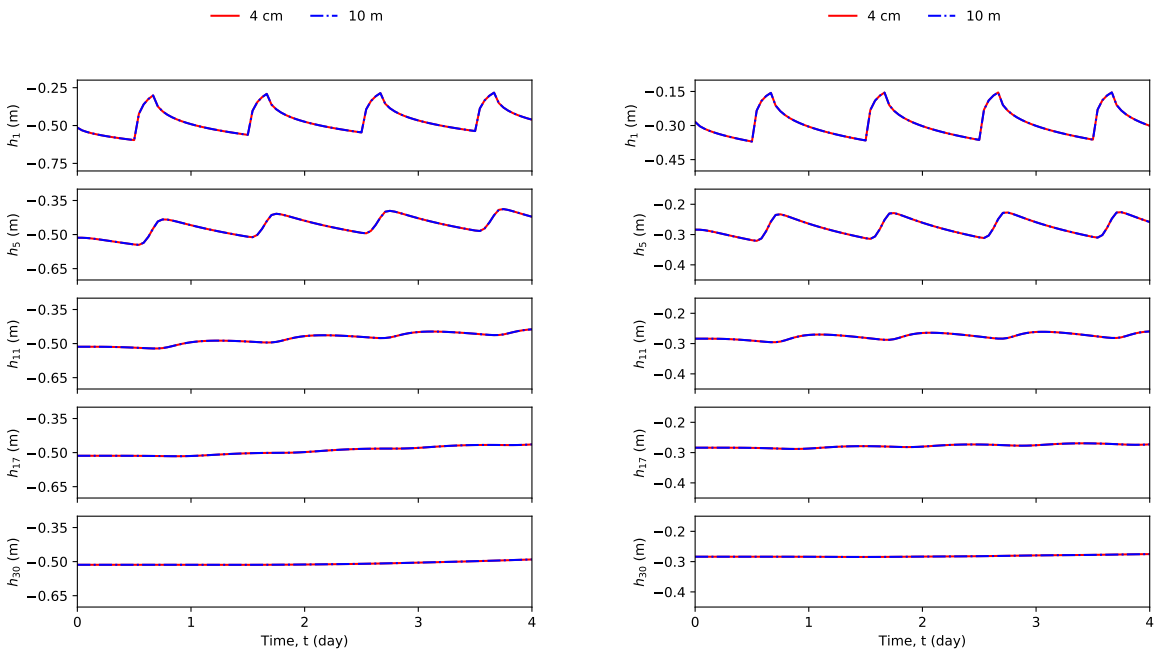

(a) Loam (b) Sandy clay loam

Figure 3.5: Comparison of selected trajectories of Model 1 (4 cm) and Model 2 (10 m) under Scenario 1.

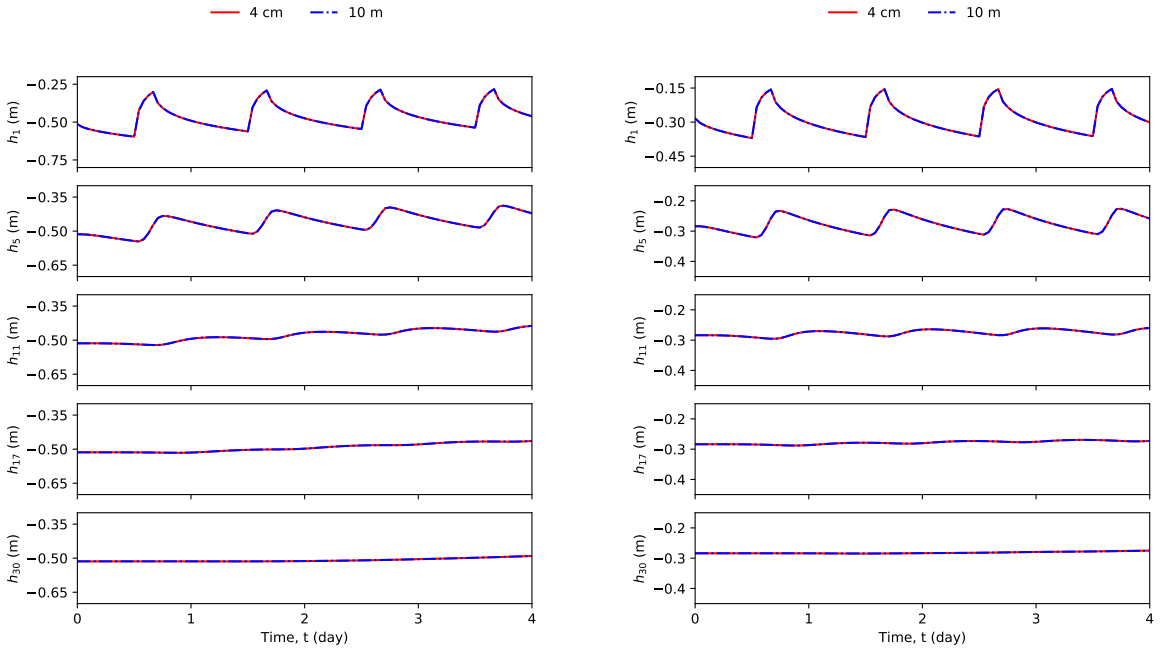

(a) Loam (b) Sandy clay loam

Figure 3.6: Comparison of selected trajectories of Model 1 (4 cm) and Model 2 (10 m) under Scenario 2.

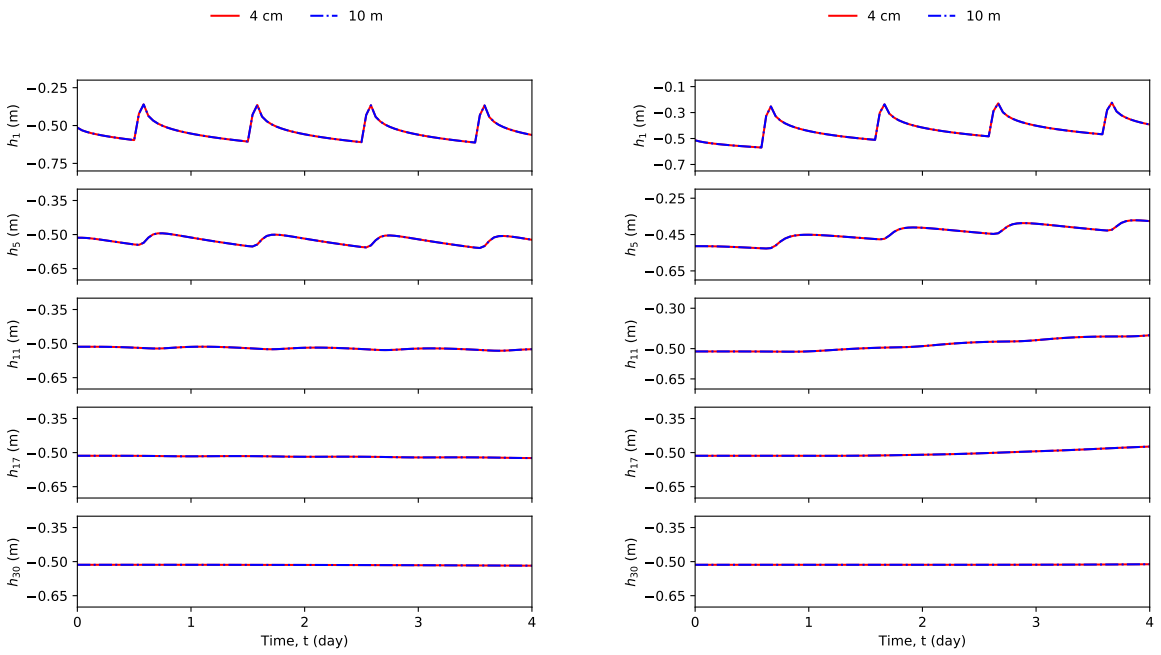

(a) Loam

(b) Sandy clay loam

Figure 3.7: Comparison of selected trajectories of Model 1 (4 cm) and Model 2 (10 m) under Scenario 3.

3.3.4 Observability Test on Subsystems

The observability of each subsystem is tested using the method introduced in Subsection 2.3. In each subsystem, the parameter set (K_s, θ_s, α, and n) is presented. According to the previous observability analysis, the augmented model with such parameter set is observable. Sensitivity analysis is not required for selecting the significant parameter set. At last, 4 sensors are the minimum number of sensors required to ensure the identifiability of selected parameters in each subsystem.

3.3.5 Decentralized Framework Motivation

In this subsection, a quantitative result is shown to support the analysis in Subsection 3.2.3 and further motivate the decentralized framework. The trajectories of the magnitudes of terms (3.10) and (3.12) are generated under Scenario 1. The 2nd top state in the left

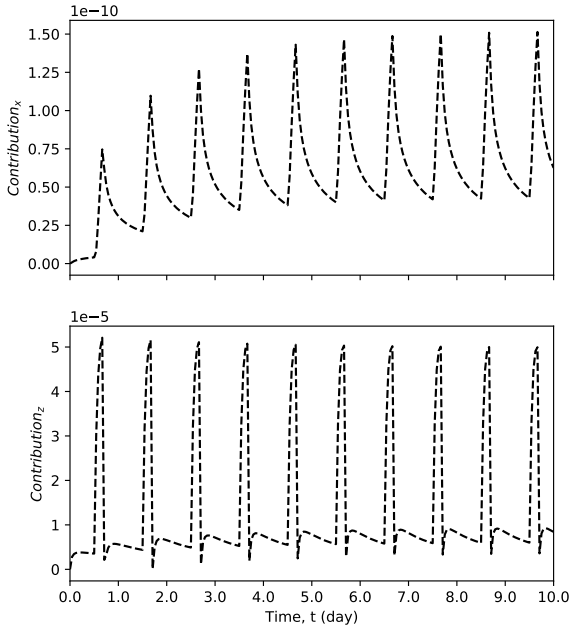

Figure 3.8: Trajectories of contributions of states in x and z directions to the system propagation.

subsystem is defined as $x_{i,j,k}$. The top figure of Figure 3.8 shows the trajectory of magnitude of term (3.10) and the bottom figure shows the trajectory of magnitude of term (3.12). They show that the magnitude of term (3.12) is around 0.5×10^6 greater than the magnitude of term (3.10). Therefore, the horizontal interactions between the states are notably smaller, comparing to the vertical interactions between the states. In other words, the interaction between the proposed subsystems are notably small. Because the information exchange between MHEs are negligible, DeMHE is justified.

3.3.6 Simultaneous Parameter and State Estimation

In this subsection, DeMHE is applied to the subsystems described in Subsection 3.3.3, to estimate their states and parameters. The performance of DeMHE is studied under the three scenarios mentioned in Subsection 3.3.3. According to the minimum number of sensors found in Subsection 3.3.4, 4 sensors are sufficient for estimating the parameters and states of

Table 3.4: True values of initial states and parameters of the process and the initial guesses used in estimators.

	Variables	True value	Initial guess
MHE 1	K_s (m/s)	2.89×10^{-6}	3.18×10^{-6}
	θ_s (m^3/m^3)	0.430	0.387
	α $(1/m)$	3.60	3.24
	n	1.56	1.72
	θ_r (m^3/m^3)	0.0780	0.0780
MHE 2	K_s (m/s)	3.64×10^{-6}	4.00×10^{-6}
	θ_s (m^3/m^3)	0.390	0.351
	α $(1/m)$	5.90	5.31
	n	1.48	1.62
	θ_r (m^3/m^3)	0.100	0.100
MHE 1 & 2	x_0 (m)	-0.514	-0.617

a subsystem. In this study, in order to ensure we can obtained enough information from the process, we assume that 8 tensiometers (N_y) are installed in each subsystem. Specifically, each type of soil is measured by 8 sensors and these sensors are installed at which the states are defined. In each soil, the sensors are installed at 5.23 cm, 13.6 cm, 22.0 cm, 30.4 cm, 38.7 cm, 47.1 cm, 55.5 cm, and 63.9 cm below the surface, which measure the 2nd, 6th, 10th, 14th, 18th, 22th, 26th and 30th states, respectively. Eight parameters (K_s, θ_s, α, and n for both loam and sandy clay loam) of the system are interested. The actual parameter values used to describe the system are shown in Table 3.1 and they are assumed to be constant within the investigated temporal domain. Process noise and measurement noise (ω_x and ν) are considered in the simulations and they have zero mean and standard deviations 3×10^{-6} m and 8×10^{-3} m, respectively.

In the design of DeMHE, MHE 1 and MHE 2 are designed for Subsystem 1 and Subsystem 2, respectively. The algorithm of MHE 1 and MHE 2 are introduced in Subsection 3.2. The initial guesses of the parameters and initial states in the estimator are listed in Table 3.4 and compared with those used in the actual system.

The designs of two MHEs are described as follows. The estimation window sizes of both MHEs are 8 hours. The weighting matrices P^n, Q^n, and R^n of both MHEs are the same. Specifically, the matrices Q^n and R^n are designed as the covariance matrices of ω_x^n and ν^n

Table 3.5: Lower and upper bounds used in DeMHE.

	Variables	Lower bounds	Upper bounds
MHE 1	$\hat{K}_s$ (m/s)	2.31×10^{-6}	3.47×10^{-6}
	$\hat{\theta}_s$ (m^3/m^3)	0.344	0.516
	$\hat{\alpha}$ (1/m)	2.88	4.32
	$\hat{n}$	1.25	1.87
MHE 2	$\hat{K}_s$ (m/s)	2.91×10^{-6}	4.37×10^{-6}
	$\hat{\theta}_s$ (m^3/m^3)	0.312	0.468
	$\hat{\alpha}$ (1/m)	4.72	7.08
	$\hat{n}$	1.18	1.78
MHE 1 & 2	$\hat{x}$ (m)	-1.00	-1.00×10^{-4}
	$\hat{\omega}_x$	-∞	∞
	$\hat{\omega}_p$	0.00	0.00

with the standard deviations mentioned in Subsection 3.3.1. The diagonal elements of Q^n corresponding to augmented parameters are 0, because the parameters are assumed to be temporally constant. In simulations, 10^{-20} is used to approximate the value 0 and to ensure the positive definiteness of Q^n. The diagonal elements of P^n corresponding to the states are designed as $(3 \times 10^{-3})^2$ and those of parameters are configured as $(3 \times 10^{-2})^2$. Then by retaining the same ratio with respect to the matrices described before, P^n, Q^n, and R^n are increased with a much bigger magnitude to ensure the numerical stability of the associated optimization problem. The P^n matrix is constant for all the optimizations. One thing worth mentioning is that even the designed weighting matrices for two MHEs are the same, the weighting matrices could be designed differently for different types of soil, especially when the parameter heterogeneity is significant. The designs of constraints of the states, parameters and the model uncertainty are listed in Table 3.5. The upper and lower bounds of the term $\hat{\omega}_p$ are 0 because the parameters are constant.

The root mean square errors, $RMSE_x$ and $RMSE_p$, are used to evaluate the performance of DeMHE on state and parameter estimation, respectively. The formulas are mentioned in Subsection 2.4.3.

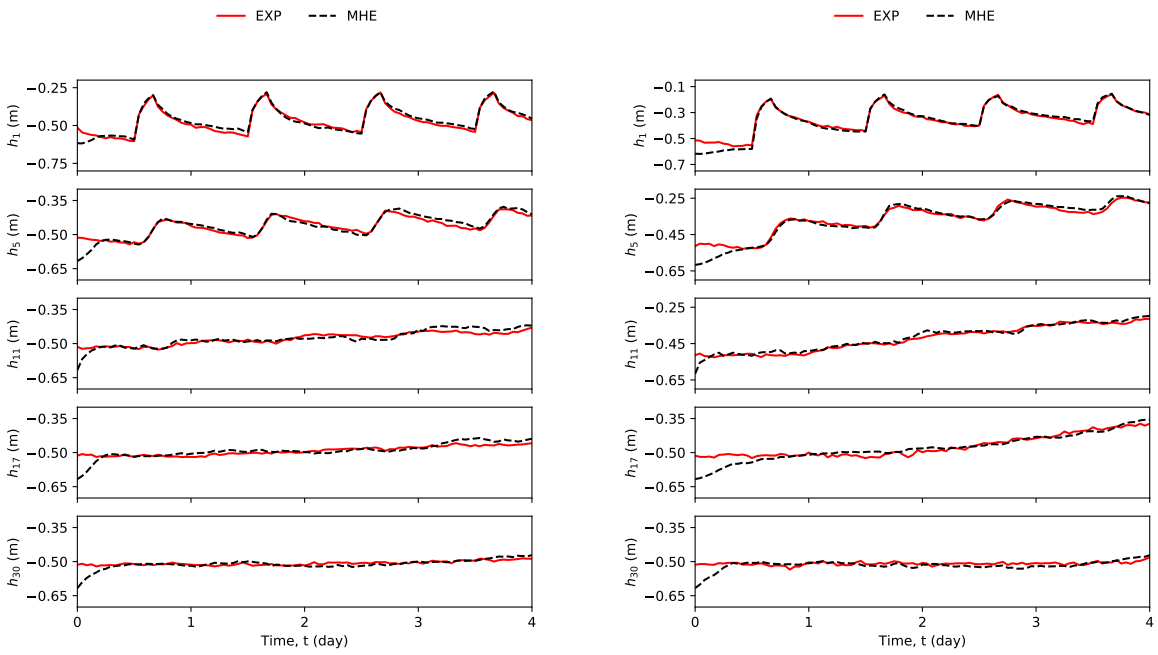

(a) Loam

(b) Sandy clay loam

Figure 3.9: Selected trajectories of the process states and estimated states using DeMHE.

3.3.6.1 Scenario 1

The DeMHE is applied to the system under Scenario 1 and its performance is assessed as the following. Figure 3.9 shows some representative estimated states and Figure 3.10 shows all estimated parameters using DeMHE. The estimated values are also compared with their true values, which are obtained using Model 1 with both Δx and Δy equaling to 4 cm. In each figure, the subplot on the left side is for loam and the one the right side is for sandy clay loam.

Figure 3.9 shows the state trajectories of the top node and a few middle nodes and one bottom node. From the figure, it can be seen that the top node has more dynamics because it takes time for irrigated water to pass from the upper part and to the lower part. In terms of state estimation performance, from Figure 3.9, it can be seen that DeMHE gives very much accurate state estimates. Note that from Figure 3.9, it can also be seen that the estimates of the 11^{th} state (h_{11}) converge faster than the other estimates. This is because it is a sensor

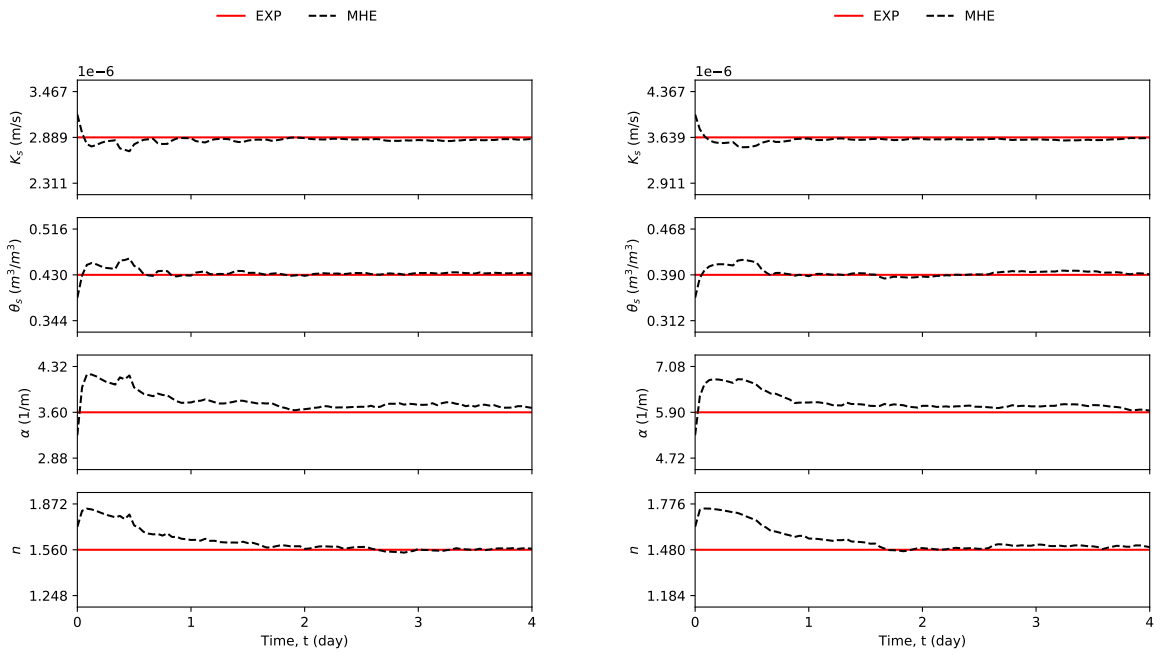

(a) Loam

(b) Sandy clay loam

Figure 3.10: Trajectories of estimated parameters using DeMHE, compared with their actual values.

node.

In terms of parameter estimation, Figure 3.10 shows the results. From the figure, it can be seen that DeMHE is capable of estimating the parameters.

These are further confirmed by Figure 3.11 that DeMHE is able to estimate states and parameters. The trajectories of the performance indices $RMSE_x$ and $RMSE_p$ associated with the DeMHE are shown in Figure 3.11 and the indices for both types of soil decrease to values less than 0.02.

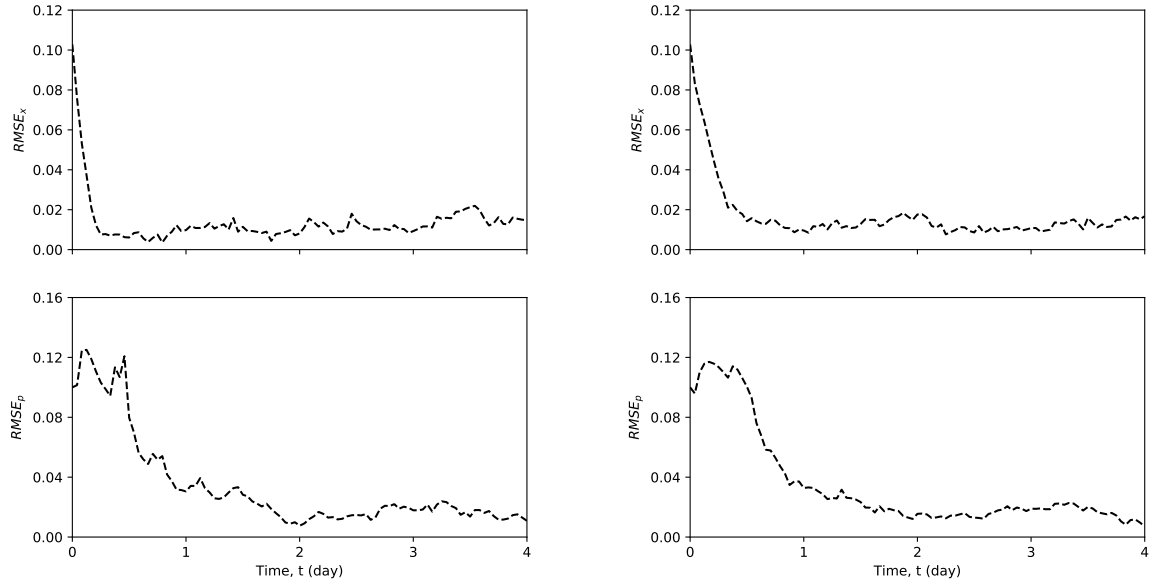

(a) Loam

(b) Sandy clay loam

Figure 3.11: Trajectories of RMSE measuring the estimation performance of DeMHE.

3.3.6.2 Scenario 2: Impact of Initial Conditions

The performance of DeMHE is assessed under Scenario 2, which is shown below. Figures 3.12 and 3.13 show some selected estimated states and all estimated parameters using DeMHE, which are also compared with their true values obtained using Model 1. As the same as before, in each figure, the subplot on the left side is for loam and the one the right side is for sandy clay loam. Figure 3.12 shows the state trajectories of the selected nodes. From the figure, not only do the trajectories of the top node have more dynamics, but also the loam and sandy clay loam are initialized at two different values. With regard to state estimation performance, it shows that DeMHE gives accurate state estimates, and the estimates of the 11^{th} state (h_{11}) converge faster than the other estimates, because it is a sensor node. Figure 3.13 compares the trajectories of estimated parameters and true parameters. It can be seen that estimated parameters converges to their true values.

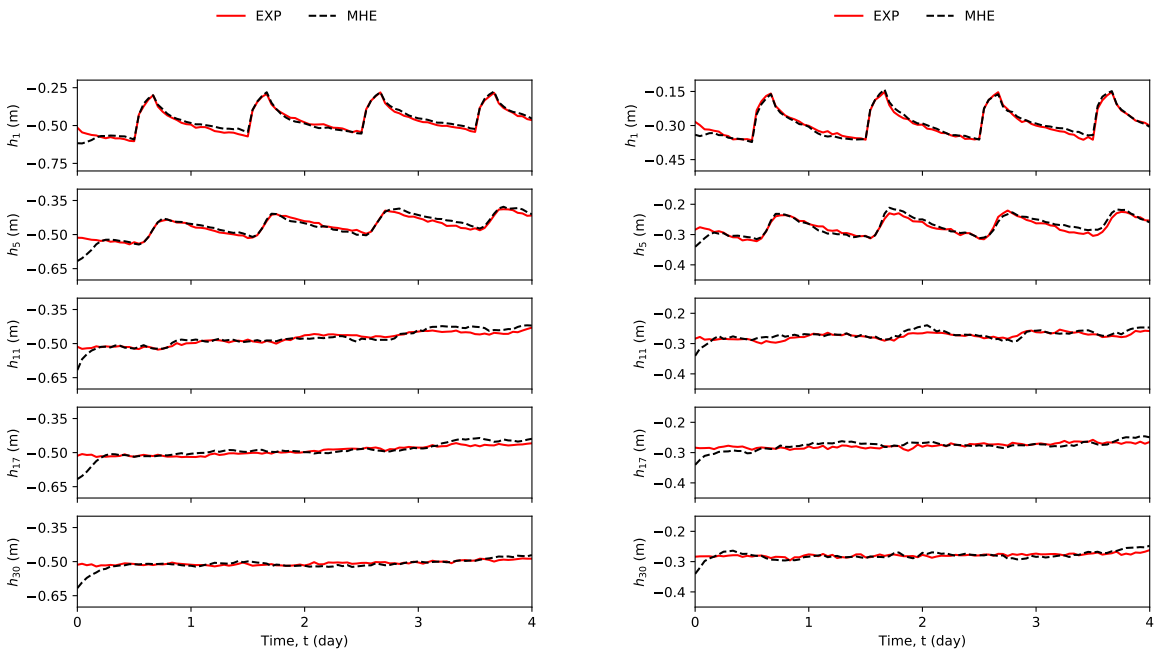

(a) Loam (b) Sandy clay loam

Figure 3.12: Selected trajectories of the process states and estimated states using DeMHE.

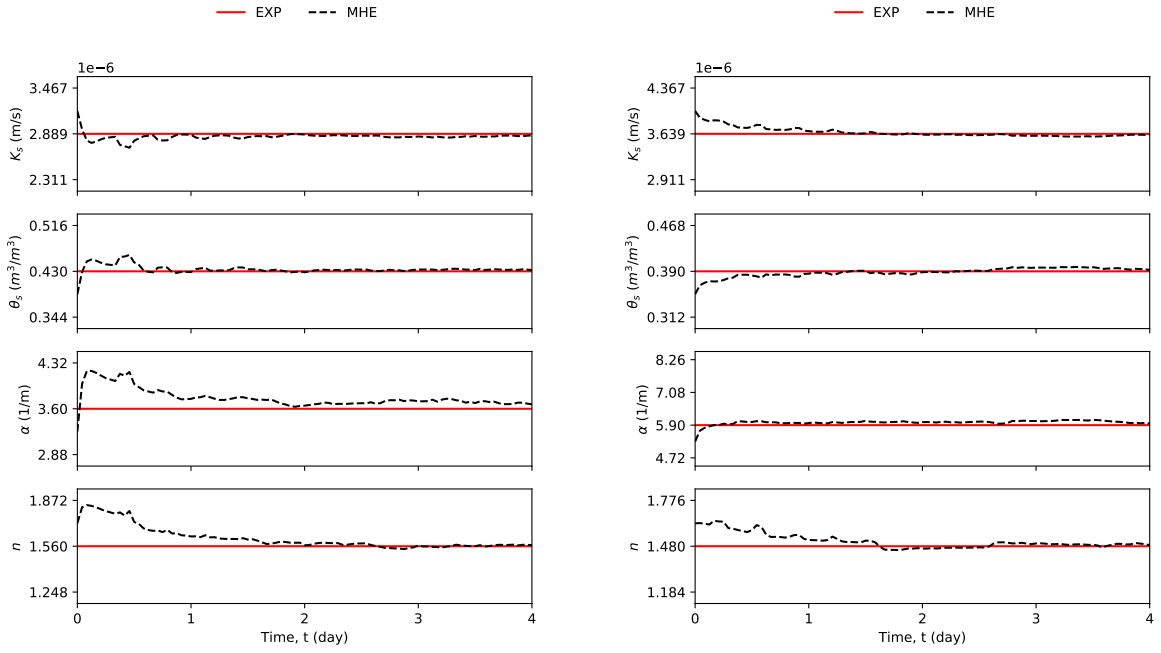

(a) Loam (b) Sandy clay loam

Figure 3.13: Trajectories of estimated parameters using DeMHE, compared with their actual values.

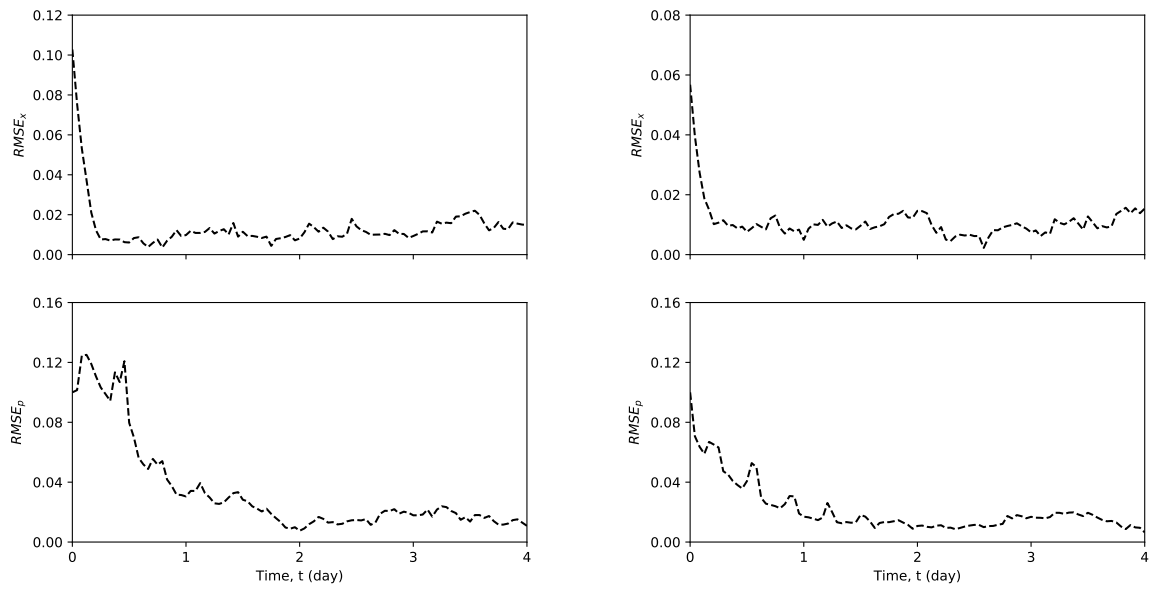

(a) Loam

(b) Sandy clay loam

Figure 3.14: Trajectories of RMSE measuring the estimation performance of DeMHE for studying impact of initial conditions.

The trajectories of the performance indices $RMSE_x$ and $RMSE_p$ associated with the DeMHE are shown in Figure 3.14. The trajectories confirms the conclusions drew before by showing that indices drop to the values less than 0.02. Therefore, under Scenario 2, the proposed initial condition has negligible effects on the performance of DeMHE.

3.3.6.3 Scenario 3: Impact of Inputs

The performance of DeMHE is examined when it is applied to the system under Scenario 3. Figures 3.15 and 3.16 show some selected estimated states and all estimated parameters using DeMHE, which are also compared with their true values obtained using Model 1. Figure 3.15 shows the state trajectories of the selected nodes. From the figure, two soils are irrigated at different time. In terms of performance of state estimation, it shows that DeMHE is able to estimate states accurately. Because h_{11} of two soils are a sensor node, their estimates converge faster than others. Figure 3.16 shows that DeMHE gives very much

accurate parameter estimates of both soils.

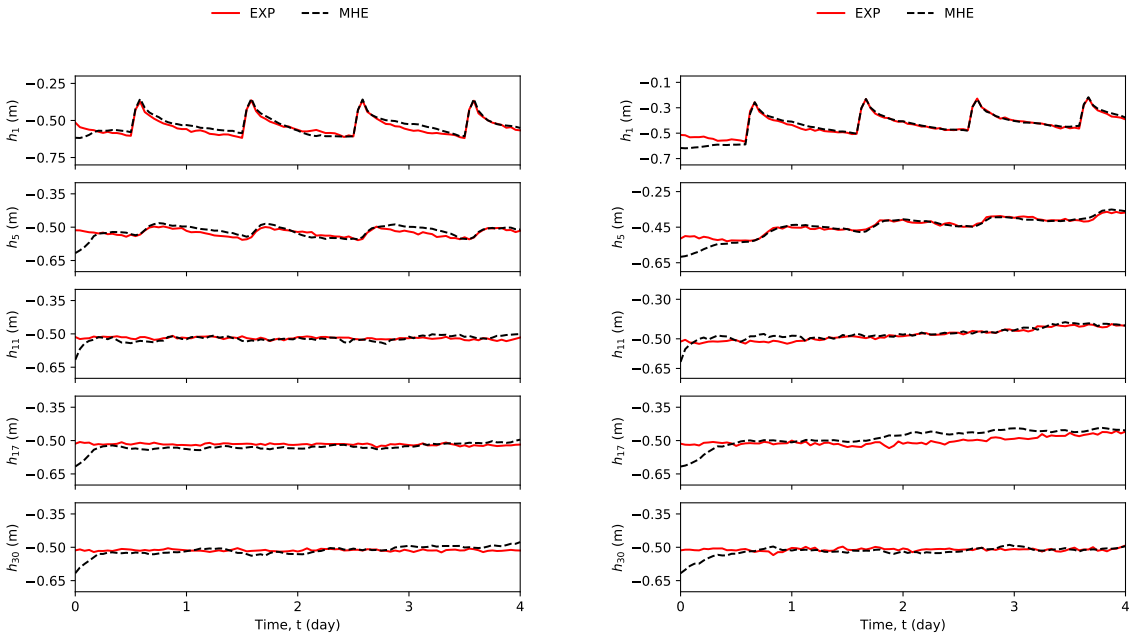

(a) Loam (b) Sandy clay loam

Figure 3.15: Selected trajectories of the process states and estimated states using DeMHE.

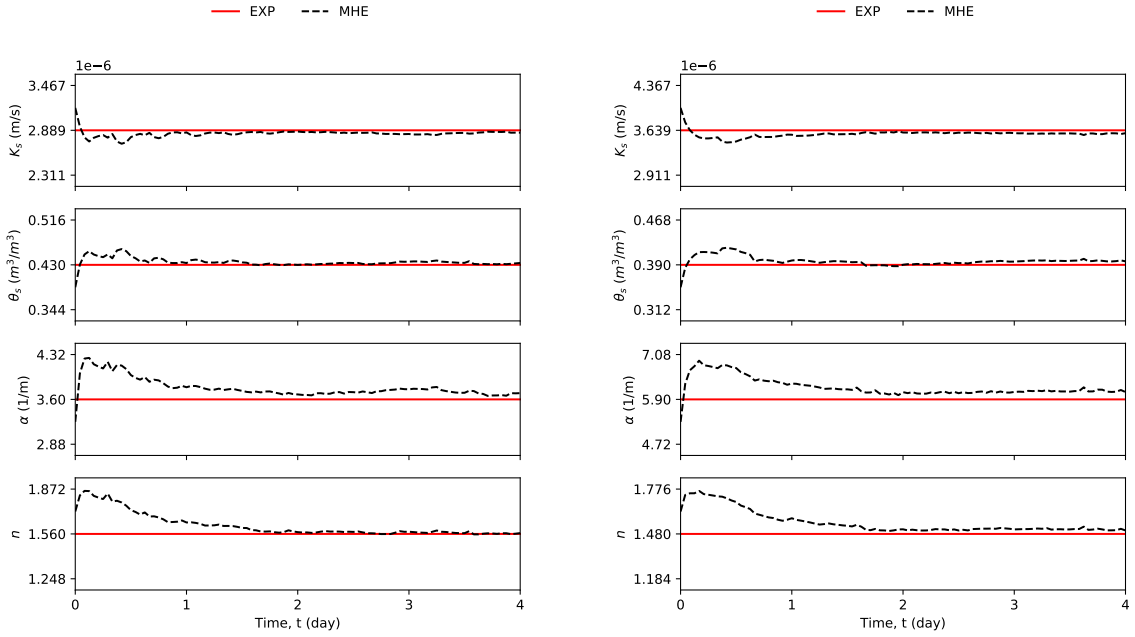

(a) Loam (b) Sandy clay loam

Figure 3.16: Trajectories of estimated parameters using DeMHE, compared with their actual values.

Figure 3.17 further confirms that DeMHE is able to estimate states and parameters. It shows the trajectories of the performance indices $RMSE_x$ and $RMSE_p$ of both types of soil associated with the DeMHE. All indices decrease to the values less than 0.02, which implies that the performance of DeMHE is not affected by the inputs proposed in Scenario 3.

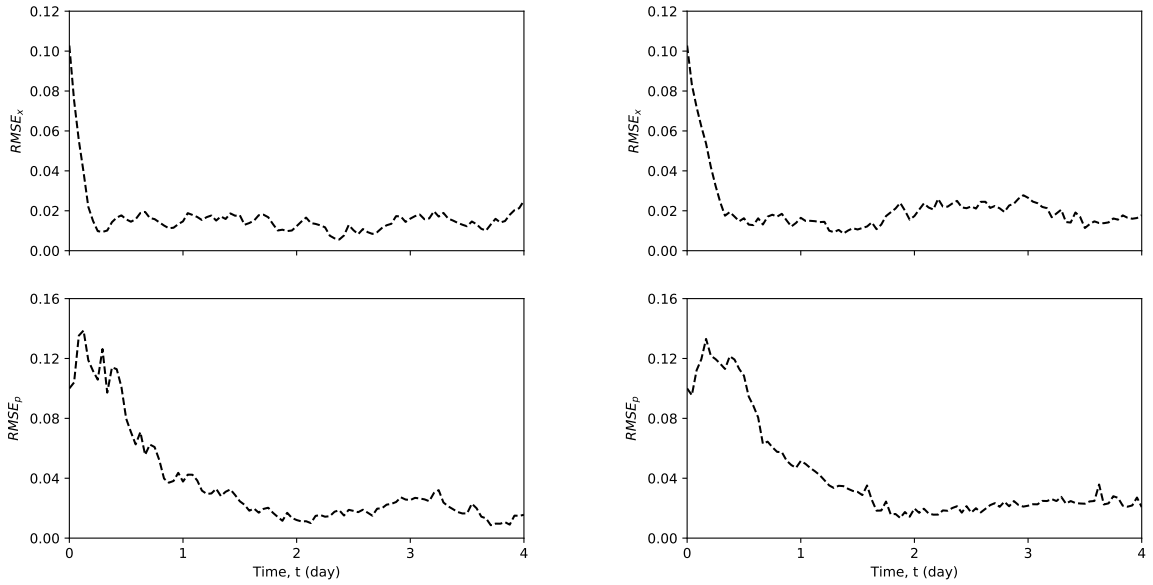

(a) Loam

(b) Sandy clay loam

Figure 3.17: Trajectories of RMSE measuring the estimation performance of DeMHE for studying impact of inputs.

3.4 Summary

In this chapter, we have investigated simultaneous state and parameter estimation using DeMHE applied to a 3D infiltration system with two types of soil. The augmented finite difference model of 3D Richards equation was constructed for simultaneous state and parameter estimation. The appropriate parameter set which contains significant and identifiable parameters was determined based on the observability of the augmented system and the sensitivity of the outputs to the parameters. It was found that the augmented system was unobservable when a pair of saturated soil moisture and residual soil moisture of the same

type of soil presented in the system. The less important parameters (residual soil moistures of both soils) were not considered in parameter estimation. Before applying DeMHE, the system was decomposed into two subsystems based on the soil types presented in the system. Each subsystem contained only one type of soil, hence, four parameters (hydraulic conductivity, saturated soil moisture, and van Genuchten-Mualem parameters). The performance of DeMHE was evaluated under the following scenarios: (1) the initial states and the inputs of two subsystems were the same; (2) the initial states of two subsystems were different, however, the inputs were the same; and (3) the inputs were different, however, the initial states were the same. The simulated results showed that DeMHE was able to estimate the states and parameters under these scenarios.

Chapter 4

Conclusions and Future work

4.1 Conclusions

In this thesis, simultaneous parameter and state estimation of 1D and 3D infiltration processes was studied.

In Chapter 2, the simultaneous parameter and state estimation was investigated using MHE, EKF and EnKF applied to an 1D infiltration system with spatially and temporally homogeneous parameters. The simultaneous estimation was achieved based on treading parameters as states by augmenting parameters at the end of the state vector. First, a procedure was proposed to find the appropriate parameter set for estimation based on the observability of the augmented system and the sensitivity of the outputs to the parameters. It was found that only four out of five parameters (hydraulic conductivity, saturated soil moisture, and van Genuchten-Mualem parameters) can be considered in simultaneous parameter and state estimation. The less important parameter (residual soil moistures) was not considered in parameter estimation. After determining the parameter set for estimation, the minimum number of sensors was also found based on the maximum multiplicity theory. Simulation results showed that the MHE has an overall the best state and parameter estimation performance due to the inclusion of parameter and state constraints in the

estimation. It was also found that the uncertainty in the residual soil moisture (which was not estimated) does not affect the overall estimation performance too much. The effects of number of measurements and estimation window size of the MHE were also studied through simulations. It was found that four measurements and a window size of eight for MHE are sufficient to provide accurate parameter and state estimates.

In Chapter 3, the simultaneous parameter and state estimation was examined using DeMHE applied to a 3D infiltration system with spatially heterogeneous parameters. The augmented finite difference model of 3D Richards equation was constructed for estimating the parameters and states of the system simultaneously. The appropriate parameter set which contains significant and identifiable parameters was determined based on the observability of the augmented system and the sensitivity of the outputs to the parameters. It was found that the augmented system was unobservable when a pair of saturated soil moisture and residual soil moisture of the same type of soil was presented in the system. With the sensitivity analysis showing the residual soil moisture was less important than the saturated soil moisture which is from the same soil, residual soil moistures of all presented soils were not considered in parameter estimation. In order to apply DeMHE, the system was decomposed into subsystems based on the soil types presented in the system. Each subsystem contained only one type of soil, hence, only four parameters (hydraulic conductivity, saturated soil moisture, and van Genuchten-Mualem parameters) of the same type of soil presented in each subsystem. The performance of DeMHE was evaluated under the following scenarios: (1) the initial states and the inputs of subsystems were the same; (2) the initial states of subsystems were different, however, the inputs were the same; and (3) the inputs were different, however, the initial states were the same. The simulated results showed that DeMHE was able to estimate the parameters and states under these scenarios.

4.2 Future Work

- *Parameter and state estimation of infiltration processes using soil moisture measurements* Besides the usage of the tensiometer in agriculture, the soil moisture sensor which direct provides volumetric soil moisture readings is also widely used. When the soil moisture is considered as the output of the system, the output function becomes a nonlinear function of the states and parameters (saturated and residual soil moistures and van Genuchten-Mualem parameters). This makes the estimation problem more complicated, hence, worth being studied.

- *Parameter and state estimation of agro-hydrological systems* The agro-hydrological system describes the water movements between soil, crop and atmosphere. In this thesis, the infiltration process modeled by Richards equation only covers the water dynamics within soil. In the future work, evapo-transpiration model and crop growth model, which are used to calculated the evapo-transpiration value for different crops at different growth states, can be incorporated with Richards equation. The parameter and state estimation problem can be studied on a completed agro-hydrological system.

Bibliography

[1] Aquastat main database. food and agriculture organization of the united nations (fao). website accessed on oct. 31, 2019.

[2] G. Fischer, F. N. Tubiello, H. van Velthuizen, and D. A. Wiberg. Climate change impacts on irrigation water requirements: Effects of mitigation, 1990–2080. *Technological Forecasting and Social Change*, 74(7):1083–1107, 2007.

[3] Y. Mao, S. Liu, J. Nahar, J. Liu, and F. Ding. Soil moisture regulation of agro-hydrological systems using zone model predictive control. *Computers and Electronics in Agriculture*, 154:239–247, 2018.

[4] A. Narasingam, P. Siddhamshetty, and J. S. I. Kwon. Handling spatial heterogeneity in reservoir parameters using proper orthogonal decomposition based ensemble kalman filter for model-based feedback control of hydraulic fracturing. *Industrial & Engineering Chemistry Research*, 57(11):3977–3989, 2018.

[5] S. I. Aanonsen, G. Nævdal, D. S. Oliver, A. C. Reynolds, B. Vallès, et al. The ensemble kalman filter in reservoir engineering–a review. *SPE Journal*, 14(03):393–412, 2009.

[6] P. Siddhamshetty and J. S. I. Kwon. Model-based feedback control of oil production in oil-rim reservoirs under gas coning conditions. *Computers & Chemical Engineering*, 112:112–120, 2018.

[7] A. Hasan, B. Foss, and S. Sagatun. Flow control of fluids through porous media. *Applied Mathematics and Computation*, 219(7):3323–3335, 2012.

[8] L. Bengtsson, M. Ghil, and E. Källén. *Dynamic meteorology: Data assimilation methods*, volume 36. Springer, 1981.

[9] M. Ghil and P. Malanotte-Rizzoli. Data assimilation in meteorology and oceanography. In *Advances in Geophysics*, volume 33, pages 141–266. Elsevier, 1991.

[10] M. Th. van Genuchten. A closed-form equation for predicting the hydraulic conductivity of unsaturated soils. *Soil Science Society of America journal*, 44(5):892–898, 1980.

[11] D. W. Marquardt. An algorithm for least-squares estimation of nonlinear parameters. *Journal of the Society for Industrial and Applied Mathematics*, 11(2):431–441, 1963.

[12] J. B. Kool, J. C. Parker, and M. Th. van Genuchten. Determining soil hydraulic properties from one-step outflow experiments by parameter estimation: I. theory and numerical studies. *Soil Science Society of America Journal*, 49(6):1348–1354, 1985.

[13] A. F. Toorman, P. J. Wierenga, and R. G. Hills. Parameter estimation of hydraulic properties from one-step outflow data. *Water Resources Research*, 28(11):3021–3028, 1992.

[14] J. C. van Dam, J. N. M. Stricker, and P. Droogers. Inverse method for determining soil hydraulic functions from one-step outflow experiments. *Soil Science Society of America Journal*, 56(4):1042, 1992.

[15] S. I. Hwang and S. E. Powers. Estimating unique soil hydraulic parameters for sandy media from multi-step outflow experiments. *Advances in Water Resources*, 26(4):445–456, 2003.

[16] D. Russo, E. Bresler, U. Shani, and J. C. Parker. Analyses of infiltration events in

relation to determining soil hydraulic properties by inverse problem methodology. *Water Resources Research*, 27(6):1361–1373, 1991.

[17] K. C. Abbaspour, M. Th. van Genuchten, R. Schulin, and E. Schläppi. A sequential uncertainty domain inverse procedure for estimating subsurface flow and transport parameters. *Water Resources Research*, 33(8):1879–1892, 1997.

[18] A. Ritter, F. Hupet, R. Muñoz-Carpena, S. Lambot, and M. Vanclooster. Using inverse methods for estimating soil hydraulic properties from field data as an alternative to direct methods. *Agricultural Water Management*, 59(2):77–96, 2003.

[19] N. S. A. Rashid, M. Askari, T. Tanaka, J. Simunek, and M. Th. van Genuchten. Inverse estimation of soil hydraulic properties under oil palm trees. *Geoderma*, 241:306–312, 2015.

[20] Y. B. Li, Y. Liu, W. B. Nie, and X. Y. Ma. Inverse modeling of soil hydraulic parameters based on a hybrid of vector-evaluated genetic algorithm and particle swarm optimization. *Water*, 10(1):84, 2018.

[21] C. Montzka, H. Moradkhani, L. Weihermüller, H. J. H. Franssen, M. Canty, and H. Vereecken. Hydraulic parameter estimation by remotely-sensed top soil moisture observations with the particle filter. *Journal of Hydrology*, 399(3-4):410–421, 2011.

[22] H. Lü, Z. Yu, Y. Zhu, S. Drake, Z. Hao, and E. A. Sudicky. Dual state-parameter estimation of root zone soil moisture by optimal parameter estimation and extended kalman filter data assimilation. *Advances in Water Resources*, 34(3):395–406, 2011.

[23] C. Li and L. Ren. Estimation of unsaturated soil hydraulic parameters using the ensemble kalman filter. *Vadose Zone Journal*, 10(4):1205–1227, 2011.

[24] H. Medina, N. Romano, and G. B. Chirico. Kalman filters for assimilating near-surface observations into the richards equation–part 2: A dual filter approach for simultaneous

retrieval of states and parameters. *Hydrology and Earth System Sciences*, 18(7):2521–2541, 2014.

[25] H. Moradkhani, S. Sorooshian, H. V. Gupta, and P. R. Houser. Dual state–parameter estimation of hydrological models using ensemble kalman filter. *Advances in Water Resources*, 28(2):135–147, 2005.

[26] W. Chen, C. Huang, H. Shen, and X. Li. Comparison of ensemble-based state and parameter estimation methods for soil moisture data assimilation. *Advances in Water Resources*, 86:425–438, 2015.

[27] A. Chaudhuri, H. J. H. Franssen, and M. Sekhar. Iterative filter based estimation of fully 3d heterogeneous fields of permeability and mualem-van genuchten parameters. *Advances in Water Resources*, 122:340–354, 2018.

[28] C. V. Rao, J. B. Rawlings, and D. Q. Mayne. Constrained state estimation for nonlinear discrete-time systems: Stability and moving horizon approximations. *IEEE Transactions on Automatic Control*, 48(2):246–258, 2003.

[29] F. Allgöwer, T. A. Badgwell, J. S. Qin, J. B. Rawlings, and S. J. Wright. Nonlinear predictive control and moving horizon estimation–an introductory overview. In *Advances in Control*, pages 391–449. Springer, 1999.

[30] E. L. Haseltine and J. B. Rawlings. Critical evaluation of extended kalman filtering and moving-horizon estimation. *Industrial & Engineering Chemistry Research*, 44(8):2451–2460, 2005.

[31] A. Alessandri, M. Baglietto, and G. Battistelli. Receding-horizon estimation for discrete-time linear systems. *IEEE Transactions on Automatic Control*, 48(3):473–478, 2003.

[32] P. Kühl, M. Diehl, T. Kraus, J. P. Schlöder, and H. G. Bock. A real-time algorithm for

moving horizon state and parameter estimation. *Computers & Chemical Engineering*, 35(1):71–83, 2011.

[33] P. D. Christofides, R. Scattolini, D. M. de la Pena, and J. Liu. Distributed model predictive control: A tutorial review and future research directions. *Computers & Chemical Engineering*, 51:21–41, 2013.

[34] R. Scattolini. Architectures for distributed and hierarchical model predictive control–a review. *Journal of Process Control*, 19(5):723–731, 2009.

[35] P. Daoutidis, M. Zachar, and S. S. Jogwar. Sustainability and process control: A survey and perspective. *Journal of Process Control*, 44:184–206, 2016.

[36] X. Yin and J. Liu. Subsystem decomposition of process networks for simultaneous distributed state estimation and control. *AIChE Journal*, 65(3):904–914, 2019.

[37] B. T. Stewart, A. N. Venkat, J. B. Rawlings, S. J. Wright, and G. Pannocchia. Cooperative distributed model predictive control. *Systems & Control Letters*, 59(8):460–469, 2010.

[38] A. N. Venkat, J. B. Rawlings, and S. J. Wright. Stability and optimality of distributed model predictive control. In *Proceedings of the 44th IEEE Conference on Decision and Control*, pages 6680–6685. IEEE, 2005.

[39] M. Heidarinejad, J. Liu, D. M. de la Peña, J. F. Davis, and P. D. Christofides. Multirate lyapunov-based distributed model predictive control of nonlinear uncertain systems. *Journal of Process Control*, 21(9):1231–1242, 2011.

[40] W. B. Dunbar. Distributed receding horizon control of dynamically coupled nonlinear systems. *IEEE Transactions on Automatic Control*, 52(7):1249–1263, 2007.

[41] R. Halvgaard, L. Vandenberghe, N. K. Poulsen, H. Madsen, and J. B. Jørgensen. Distributed model predictive control for smart energy systems. *IEEE Transactions on Smart Grid*, 7(3):1675–1682, 2016.

[42] J. Zhang and J. Liu. Distributed moving horizon state estimation for nonlinear systems with bounded uncertainties. *Journal of Process Control*, 23(9):1281–1295, 2013.

[43] R. Vadigepalli and F. J. Doyle. A distributed state estimation and control algorithm for plantwide processes. *IEEE Transactions on Control Systems Technology*, 11(1):119–127, 2003.

[44] X. Yin, J. Zeng, and J. Liu. Forming distributed state estimation network from decentralized estimators. *IEEE Transactions on Control Systems Technology*, 27(6):2430–2443, 2019.

[45] L. Xie, D. H. Choi, S. Kar, and H. V. Poor. Fully distributed state estimation for wide-area monitoring systems. *IEEE Transactions on Smart Grid*, 3(3):1154–1169, 2012.

[46] M. Farina, G. Ferrari-Trecate, and R. Scattolini. Distributed moving horizon estimation for nonlinear constrained systems. *International Journal of Robust and Nonlinear Control*, 22(2):123–143, 2012.

[47] A. Haber and M. Verhaegen. Moving horizon estimation for large-scale interconnected systems. *IEEE Transactions on Automatic Control*, 58(11):2834–2847, 2013.

[48] X. Yin, B. Decardi-Nelson, and J. Liu. Subsystem decomposition and distributed moving horizon estimation of wastewater treatment plants. *Chemical Engineering Research and Design*, 134:405–419, 2018.

[49] R. Schneider and W. Marquardt. Convergence and stability of a constrained partition-based moving horizon estimator. *IEEE Transactions on Automatic Control*, 61(5):1316–1321, 2016.

[50] M. Farina, G. Ferrari-Trecate, and R. Scattolini. Distributed moving horizon estimation for sensor networks. *IFAC Proceedings Volumes*, 42(20):126–131, 2009.

[51] X. Yin and J. Liu. Distributed moving horizon state estimation of two-time-scale nonlinear systems. *Automatica*, 79:152 – 161, 2017.

[52] S. Bo, S. R. Sahoo, X. Yin, J. Liu, and S. L. Shah. Parameter and state estimation of one-dimensional infiltration processes: A simultaneous approach. *Mathematics*, 8(1):134, 2020.

[53] J. Nahar. *Closed-loop irrigation scheduling and control*. PhD thesis, University of Alberta, 2019.

[54] L. A. Richards. Capillary conduction of liquids through porous mediums. *Physics*, 1(5):318–333, 1931.

[55] M. B. Almendro-Candel, I. G. Lucas, J. Navarro-Pedreño, and A. A. Zorpas. Physical properties of soils affected by the use of agricultural waste. *Agricultural Waste and Residues*, page 9, 2018.

[56] G. Evensen. Sequential data assimilation with a nonlinear quasi-geostrophic model using monte carlo methods to forecast error statistics. *Journal of Geophysical Research: Oceans*, 99(C5):10143–10162, 1994.

[57] S. Gillijns, O. B. Mendoza, J. Chandrasekar, B. L. R. De Moor, D. S. Bernstein, and A. Ridley. What is the ensemble kalman filter and how well does it work? In *2006 American Control Conference*, pages 6–pp. IEEE, 2006.

[58] S. R. Sahoo, X. Yin, and J. Liu. Optimal sensor placement for agro-hydrological systems. *AIChE Journal*, 65(12):e16795, 2019.

[59] A. F. Villaverde, A. Barreiro, and A. Papachristodoulou. Structural identifiability of dynamic systems biology models. *PLOS Computational Biology*, 12(10), 2016.

[60] J. Nahar, J. Liu, and S. L. Shah. Parameter and state estimation of an agro-hydrological system based on system observability analysis. *Computers & Chemical Engineering*, 121:450–464, 2019.

[61] P. Eykhoff. *System identification: parameter and state estimation*. Wiley, London, 1974.

[62] Z. Yuan, C. Zhao, Z. Di, W. X. Wang, and Y. C. Lai. Exact controllability of complex networks. *Nature Communications*, 4(1):1–9, 2013.

[63] R. F. Carsel and R. S. Parrish. Developing joint probability distributions of soil water retention characteristics. *Water Resources Research*, 24(5):755–769, 1988.